Oceanic ventilation and biogeochemical cycling: Understanding the physical mechanisms that produce realistic distributions of tracers and productivity

Anand Gnanadesikan,[1] John P. Dunne,[1] Robert M. Key,[2] Katsumi Matsumoto,[3] Jorge L. Sarmiento,[2] Richard D. Slater,[2] and P. S. Swathi[4]

Received 23 May 2003; revised 26 March 2004; accepted 30 July 2004; published 20 October 2004.

[1] Differing models of the ocean circulation support different rates of ventilation, which in turn produce different distributions of radiocarbon, oxygen, and export production. We examine these fields within a suite of general circulation models run to examine the sensitivity of the circulation to the parameterization of subgridscale mixing and surface forcing. We find that different models can explain relatively high fractions of the spatial variance in some fields such as radiocarbon, and that newer estimates of the rate of biological cycling are in better agreement with the models than previously published estimates. We consider how different models achieve such agreement and show that they can accomplish this in different ways. For example, models with high vertical diffusion move young surface waters into the Southern Ocean, while models with high winds move more young North Atlantic water into this region. The dependence on parameter values is not simple. Changes in the vertical diffusion coefficient, for example, can produce major changes in advective fluxes. In the coarse-resolution models studied here, lateral diffusion plays a major role in the tracer budget of the deep ocean, a somewhat worrisome fact as it is poorly constrained both observationally and theoretically. *INDEX TERMS:* 4275 Oceanography: General: Remote sensing and electromagnetic processes (0689); 4532 Oceanography: Physical: General circulation; 4568 Oceanography: Physical: Turbulence, diffusion, and mixing processes; 4845 Oceanography: Biological and Chemical: Nutrients and nutrient cycling; *KEYWORDS:* biogeochemical cycles, particle export, vertical exchange

Citation: Gnanadesikan, A., J. P. Dunne, R. M. Key, K. Matsumoto, J. L. Sarmiento, R. D. Slater, and P. S. Swathi (2004), Oceanic ventilation and biogeochemical cycling: Understanding the physical mechanisms that produce realistic distributions of tracers and productivity, *Global Biogeochem. Cycles*, *18*, GB4010, doi:10.1029/2003GB002097.

1. Introduction

[2] General circulation models (GCMs) have come to play an increasingly important role in the prediction of changes in climate and biogeochemical cycling resulting from human activity and natural variability. In the last 2 decades, the oceanographic modeling community has sought to use biogeochemical data sets to evaluate model performance. Early work was mainly focused on showing that the models could capture broad-scale features of fields such as radiocarbon [*Toggweiler et al.*, 1989; *Maier-Reimer*, 1993] and nutrients [*Najjar et al.*, 1992]. More recently, however, the community has begun to use such tracers as means of identifying specific deficiencies in models. *Toggweiler and Samuels* [1993] used radiocarbon to argue that models were upwelling too much deep waters in the equatorial zone. *England* [1995] used the distribution of CFC-11 to argue that models without eddy-induced advection produced a Southern Ocean that was excessively well mixed. *Gnanadesikan* [1999b] made a similar argument using estimates of the export of biogenic silica. However, as pointed out by *Dixon et al.* [1996], it can be difficult to compare different simulations of the same tracer if key details of the simulation (gas exchange, chemistry, etc.) are not the same across different models.

[3] The second phase of the Ocean Carbon Model Intercomparison Program (OCMIP2) was designed to attack this problem by developing standard simulation protocols for CFCs, the abiotic carbon cycle, and the biotic carbon cycle. Runs made with these protocols have found interesting differences between models. For example, *Dutay et al.* [2002] found that different OCMIP2 GCMs had quite different patterns of the penetration of CFC11 into the deep ocean, particularly the Southern Ocean. *Watson et al.* [2003] showed that the models have significantly different air-sea fluxes of carbon dioxide. *Matsumoto et al.* [2004] docu-

[1]NOAA/Geophysical Fluid Dynamics Laboratory, Princeton, New Jersey, USA.
[2]Atmospheric and Oceanic Sciences Program, Princeton University, Princeton, New Jersey, USA.
[3]Agency of Industrial Science and Technology, Geological Survey of Japan, Tsukuba, Japan.
[4]CSIR Centre for Mathematical Modeling and Computer Simulation, National Aerospace Laboratory, Bangalore, India.

0886-6236/04/2003GB002097$12.00

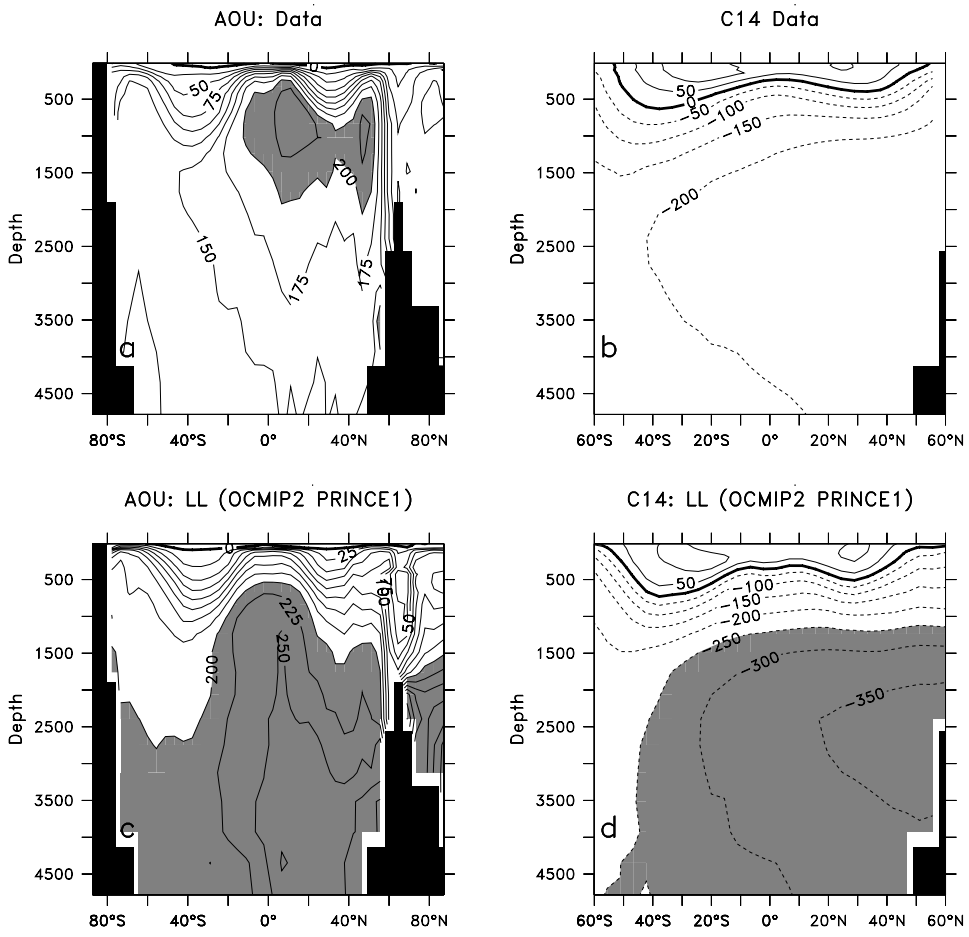

Figure 1. Illustration of poor ventilation of the deep ocean in the LL (OCMIP2 PRINCE1) model. (a) Zonally averaged AOU from the World Ocean Atlas 2001 [*Conkright et al.*, 2002]. Shading shows values great than 200 μmol/L. (b) Zonally averaged radiocarbon from the WOCE data set in the Pacific. (c) Zonally averaged AOU from LL biotic simulation. (d) Zonally averaged radiocarbon in the Pacific from LL historical simulation (year shown is 1995). Shading shows values less than −250‰, not seen in zonally averaged observations.

mented significant differences in simulations of radiocarbon. Taken together, the tracer simulations point to large differences in the rate of ventilation of the deep ocean. The physical mechanisms underlying intermodel differences, however, have remained obscure.

[4] One way of ensuring sufficient deep ventilation is to include mechanisms that enhance rates of vertical exchange in the low latitudes. Examination of the models run during OCMIP [*Doney et al.*, 2004] shows that almost all the models include such mechanisms. Some have rates of vertical diffusion significantly larger than the 0.1–0.15 cm^2/s seen in the real ocean [*Ledwell et al.*, 1993]. Others use horizontal diffusion, which allows for diapycnal transfer across sloping isopycnals [*Veronis*, 1975; *Griffies et al.*, 1998]. Two groups advect passive tracers using an upwind scheme, a numerical scheme that produces greatly enhanced numerical diffusion [*Maier-Reimer*, 1993; *Griffies et al.*, 2000]. One group restores internal temperatures and salinities toward observations, essentially guaranteeing diapycnal fluxes in the deep ocean when there are mismatches between the models and data. All in all, of the 11 models discussed by *Doney et al.* [2004] only two (the Southampton Oceanography Centre and our own Princeton model) have low diapycnal diffusion and relatively non-diffusive numerics.

[5] In our previous work [*Gnanadesikan et al.*, 2002] (hereinafter GSGS) we considered the rate of biological cycling associated with our low-diffusion model, together with an associated suite of models designed to examine the sensitivity of the ocean overturning and biological cycle to changes in the lateral and vertical diffusion. Our model (KVLOW + AILOW in GSGS) has the problem (shown in Figure 1) that it does not produce very realistic distributions of radiocarbon and oxygen. While the observed zonally averaged radiocarbon all lies above −245‰, almost the entire deep Pacific lies below this value in the model, indicating that the rate of ventilation is too slow. Most of the deep Pacific has far too high a level of apparent oxygen utilization as well.

[6] Other models in the suite reported in GSGS have higher rates of diapycnal mixing. These models simulate more realistic values of AOU and radiocarbon in the deep ocean (Figures 2a and 2c). The fact that increasing new

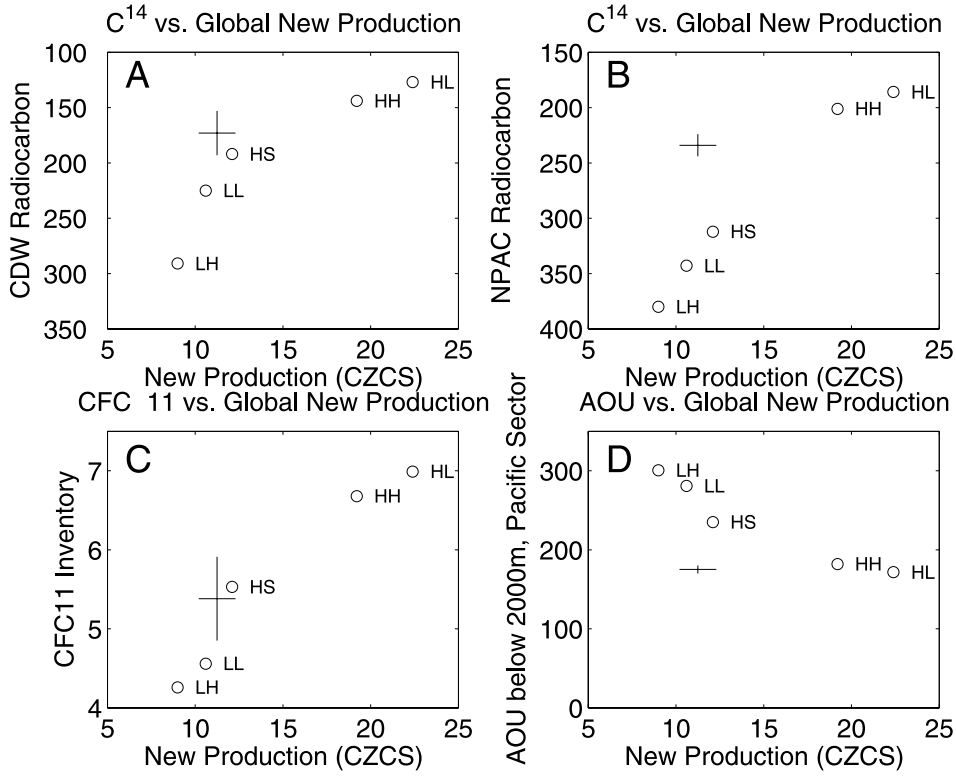

Figure 2. Water mass tracers and new production (GSGS) simulations run using the OCMIP2 protocols. The range of observational estimates is shown by the crosses. Symbols are defined in section 2 and refer to the range of models run in GSGS. (a) Radiocarbon in Circumpolar Deep Water (south of 30°S, below 1365 m) versus new production, (b) Radiocarbon in the North Pacific versus new production (from 25°N–60°N, 110°W–250°W, below 1365 m). (c) CFC-11 inventory in (10^8 mol) versus global new production. (d) Apparent oxygen utilization below 2000 m in the Pacific sector versus new production. Note that increasing new production means increasing oxygen utilization at depth, so the negative correlation is evidence of increasing ventilation.

production (which results in great oxygen consumption at depth) is correlated with decreasing AOU in this suite shows that the improvement in AOU is a result of an increase in the rate of ventilation. The results in Figure 2 present somewhat of a conundrum: While high rates of diapycnal mixing in the pycnocline appear to be necessary to produce sufficient deep ventilation, large diapycnal mixing coefficients are not consistent with observations. Nor, as reported in GSGS, are they consistent with the relatively low rates of new production (the rate of biological production driven inorganic nutrients rather than from recycled organic matter) inferred from the CZCS satellite. In the past year, we have acquired access to new gridded data sets for water mass tracers and developed new algorithms for estimating the rate of biological cycling. This makes it opportune to revisit the following questions: (1) How much of a constraint on the pathways of deep ocean ventilation is the distribution of radiocarbon? (2) In particular, to what extent is it possible to get the right answer for the wrong reasons? (3) To what extent does Figure 2 imply that models require a high mixing coefficient? (4) How robust is the constraint on the circulation resulting from satellite estimates of biological cycling?

[7] An important motivation for this work comes from a simple analytic model of the ocean overturning circulation, a schematic of which is shown in Figure 3, proposed by *Gnanadesikan* [1999a]. In this model, the pathways of oceanic circulation are predicted using a cubic equation in the pycnocline depth D. Within this equation, increasing the vertical diffusion coefficient (K_v) results in an increase in tropical upwelling and a decrease in the net upwelling within the Southern Ocean. Increasing the lateral diffusion coefficient (A_I) results in an increase in the net tropical upwelling and a decrease in the net Southern Ocean upwelling. This is because the lateral diffusion coefficient in the models diffuses not only passive tracers, but layer thickness [*Gent and McWilliams*, 1990], which results in a net advective flux of light waters into the Southern Ocean. One implication of this equation was that by changing the magnitude of the two diffusion coefficients together, one could maintain a constant pycnocline depth, and hence keep the Northern Hemisphere overturning circulation constant while changing the pathways of diapycnal transformation and upwelling between the Southern Ocean and the tropics. GSGS examined a suite of models designed to test this idea and found it to be quite accurate. More recent work by

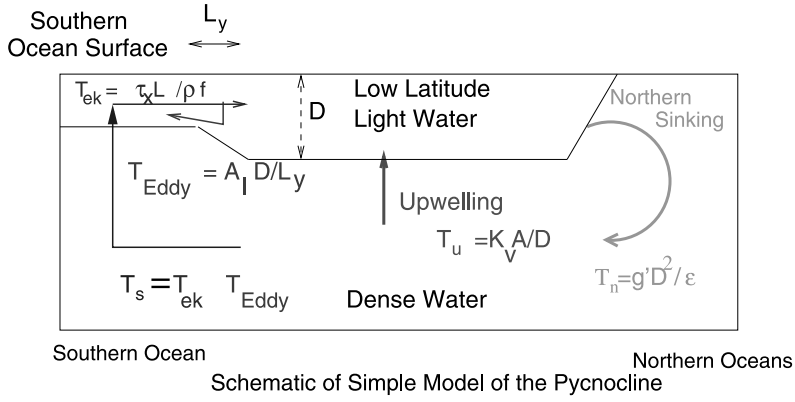

Figure 3. Schematic of the simple model of thermohaline overturning of *Gnanadesikan* [1999a]. Figure is taken from *Gnanadesikan et al.* [2003]. The figure shows four fluxes. The formation of North Atlantic Deep Water is represented by a Northern Hemisphere overturning flux T_n which goes as $g'D^2/\varepsilon$ where g' is the reduced gravity between light and dense water spheres, D is the depth of the pycnocline, and ε is a frictional resistance. This flux may be balanced either by an upwelling flux in tropical latitudes $T_u = K_v A/D$ (where K_v is the diapycnal diffusion coefficient and A is the area of the tropics) or by a Southern Ocean upwelling flux. The Southern Ocean flux is the difference between the Ekman flux $T_{ek} = \tau_x L_x/\rho f$ (where τ_x is the wind stress, L_x is the length of a latitude circle in the Southern Ocean, ρ is density and f is a scale value for the Coriolis parameter) and an eddy flux $T_{eddy} = A_I D/L_y$ (where A_I is a lateral diffusion coefficient and L_y is the scale over which the pycnocline shallows in the south). See color version of this figure at back of this issue.

Klinger et al. [2003] and *Gnanadesikan et al.* [2003] has given further support to the theory. An important finding of GSGS was that certain measures of the rate of biogeochemical cycling were more sensitive to changes in the parameterization of subgridscale mixing than were the zonally averaged temperature and salinity fields. This suggested that biogeochemical tracers could provide important information about the circulation that would otherwise be missed by concentrating on temperature and salinity alone.

[8] In this paper, we demonstrate that while radiocarbon, oxygen utilization, and particle export can be used to identify deficiencies in GCMs, they do not necessarily constrain how to solve such deficiencies. As is the case with active tracers like temperature and salinity, different circulations can produce quite similar passive tracer fields. After describing the models in section 2, we discuss their relative skill at simulating particle export, radiocarbon, and oxygen in section 3, and show that the agreement between models and data is much better than would be inferred from GSGS. In section 4, we examine why the models improve, looking at the budgets of radiocarbon and oxygen in detail. We show that changing the vertical and horizontal mixing produces changes in the model budgets that are understandable in terms of a simple analytical theory. We also demonstrate that increasing vertical mixing is not the only way of improving deep ventilation, but that changing the surface boundary conditions can also have a major impact.

2. Methods

2.1. Circulation Model Description

[9] We present results from seven models, five from the suite presented in GSGS and two new simulations. All are coarse-resolution, 4° general circulation models based on the Modular Ocean Model, Version 3 code of *Pacanowski and Griffies* [1999]. All are forced with monthly-varying climatological fluxes of heat, salt, and momentum, as well as diagnosed flux corrections of heat and salt computed by restoring the surface temperatures and salinities back toward the observations collected by *Levitus et al.* [1994]. The monthly heat and salt fluxes for all the models (except for model P2A, as described below) are taken directly from the climatology of *Da Silva et al.* [1994]. Additionally, a representation of the biological cycle of phosphate and carbon is included, as specified by the OCMIP protocols and described in GSGS. All models were run out to equilibrium. Differences between the models are summarized in tabular form in Table 1. The models are as follows:

[10] 1. The LL model is the KVLOW + AILOW case from GSGS. This model has been found to have a good temperature, salinity, and pycnocline structure, reasonable globally integrated rates of uptake of anthropogenic CO_2 and CFCs but very low values of deep radiocarbon [*Matsumoto et al.*, 2004].

[11] 2. The HH model is the KVHIGH + AIHIGH case from *Gnanadesikan et al.* [2002].The lateral mixing coefficient was increased from 1000 to 2000 m^2/s and the vertical mixing coefficient within the pycnocline was increased from 0.15 to 0.6 cm^2/s. These changes were made together so as to preserve the shape of the pycnocline while shifting the pathway of deep upwelling from the Southern Ocean to low latitudes, following the theory of *Gnanadesikan* [1999a]. A major deficiency of this model is that the vertical mixing coefficient is far larger in the tropical pycnocline than can be supported by direct measurements [*Ledwell et al.*, 1993].

Table 1. Tabular Description of Four of the Seven Models[a]

	LL	HH	P2	P2A
Pycnocline diffusivity (tropics)	0.15	**0.6**	**0.3**	0.15
Pycnocline diffusivity (Southern Ocean)	0.15	**0.6**	**1.0**	**1.0**
Enhanced diffusivity in top 50 m	No	No	No	**Yes**
Lateral diffusivity	1000	**2000**	1000	1000
Applied Surface Fluxes	*Da Silva et al.* [1994]	*Da Silva et al.* [1994]	*Da Silva et al.* [1994]	*Da Silva et al.* [1994] plus **correction globally**
Temperature and salinity toward which restoring occurs	*Levitus et al.* [1994]	*Levitus et al.* [1994]	*Levitus et al.* [1994] plus **correction near Antarctica in winter**	*Levitus et al.* [1994] plus **correction near Antarctica in winter**
Wind stress	Hellermann	Hellermann	Hellermann	**ECMWF**
Topography	Wide Drake Passage	Wide Drake Passage	Wide Drake Passage	**Narrow Drake Passage**

[a]Key differences from LL are shown in bold. Model LH is identical to LL except that lateral diffusivity is increased to 2000. Model HL is similarly identical except that vertical diffusivity is increased to 0.6. Model HSL is identical except that vertical diffusivity within the Southern Ocean is changed to 1.0.

[12] 3,4. The HL and LH models have either the vertical (HL) or lateral diffusion (LH) coefficients increased to the values in HH. This enables us to examine which aspects of the changes are produced by vertical diffusion and which by lateral diffusion.

[13] 5. The HSL model has higher vertical mixing within the Southern Ocean, based on the observations of *Polzin* [1999] that internal wave activity is much higher there.

[14] 6. The P2 model uses HSL as a base. As can be seen from Figure 2, HSL struck the best compromise between fidelity to the global new production and radiocarbon numbers, though the deep ocean was still not ventilated enough. Two major alterations were made to this model to try to improve the deep radiocarbon concentrations in the North Pacific. The first was to force the model to form deep water in the Ross and Weddell Seas by imposing a strong restoring to the salinities found in bottom water at four points during the 3 months of winter. It was found that in the *Levitus et al.* [1994] data set, toward which the models in GSGS were restored, the deep water found at 200–400 m in the Weddell and Ross Seas never outcropped at the surface. Since it is well known that these waters do in fact outcrop during the winter in coastal polynyas [*Foster and Carmack*, 1976; *Fahrbach et al.*, 1994], it seemed reasonable to force the formation of such water masses at a few points. This change was found to increase deep water values of radiocarbon by 60‰, reducing the observed mismatch by about half. Since case HH showed us that a large increase in vertical diffusion coefficient could increase deep-water radiocarbon concentrations, we decided to investigate the impacts of a small increase in vertical diffusivity. We thus increased the vertical diffusion coefficient within the low-latitude pycnocline from 0.15 cm^2/s to 0.3 cm^2/s. This latter value is significantly larger than that found by *Ledwell et al.* [1993]. However, it is identical to that used in previous versions of the POBM [*Najjar et al.*, 1992; *Gnanadesikan*, 1999b].

[15] 7. The P2A model, like P2, has boundary conditions that were altered in the far Southern Ocean to increase the formation of deep dense water. However, in contrast to P2, this model attempts to resolve the radiocarbon problem without increasing the vertical diffusion coefficient in the pycnocline. Instead, a series of changes were made to make the Southern Ocean circulation more "realistic" (at least putatively). The wind stress field was changed from *Hellerman and Rosenstein* [1983] to the ECMWF reanalysis of *Trenberth et al.* [1989]. The zonally averaged differences in the wind stress are shown in Figure 4a. The Drake Passage, which was too broad in all the previous models (where the topography was adopted from the old GFDL coupled model) was narrowed by one grid point (~450 km). Finally, analysis of the LL model showed that the flux corrections calculated from restoring and the applied fluxes were operating in the opposite direction throughout much of the Southern Ocean (Figure 4b). This implies that the surface waters in LL are too fresh. The applied fluxes are quite uncertain (they are not, for example, globally balanced). We decided to adjust the applied fluxes by adding the flux corrections computed from restoring. As can be seen from Figure 4b, this substantially reduces the applied freshwater flux to the Southern Ocean. The result of this change is to destabilize the surface, allowing for more deep ventilation.

2.2. Data Sets With Which the Models are Compared

[16] Comparisons are made between the models and four data sets, three of which are new. Apparent oxygen utilization, phosphate, and oxygen are compared to the *Conkright et al.* [2002] World Ocean Atlas 2001. Radiocarbon is compared to a new gridded data set compiled from WOCE and GEOSECS data (R. M. Key et al., A global ocean carbon climatology: Results from GLODAP, submitted to *Global Biogeochemical Cycles*, 2004). CFC-11 is compared against a new gridded data set compiled by *Willey et al.* [2004].

[17] Additional comparisons are made with estimates of particle export made from satellite-based estimates of chlorophyll concentration based on ocean color. Particle export is the fraction of total uptake of nutrients by phytoplankton (primary productivity) that is exported as sinking particles. Previous work [*Laws et al.*, 2000] assumed that the particle export was the same as the new production (that part of the primary production fueled by upwelled nitrate from below the euphotic zone as opposed to recycled nitrogen in the form of ammonia, urea, or dissolved organic matter). We do not. We use the empirical regression of J. P. Dunne et al. (Empirical and mechanistic models of particle export, submitted to *Global Biogeochemical Cycles*, 2004) (here-

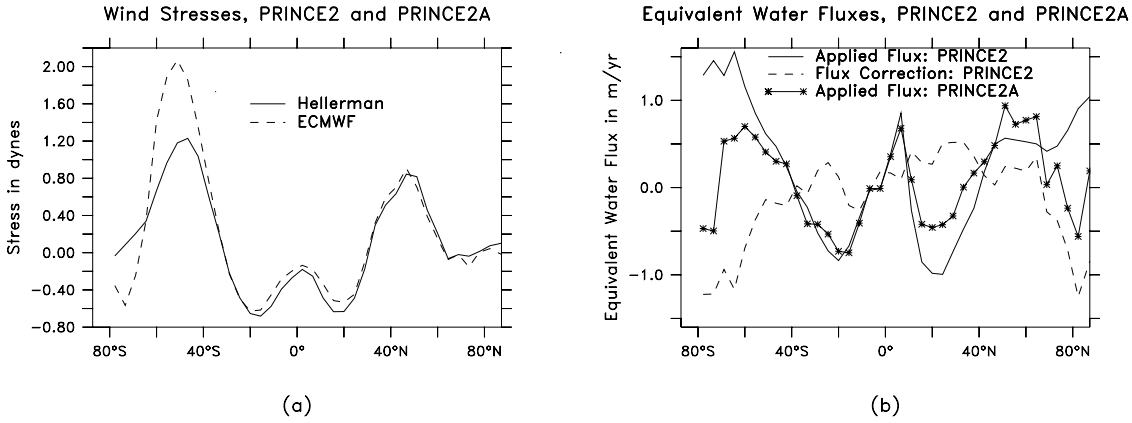

Figure 4. Changes in surface fluxes between P2 and P2A. (a) Wind stresses. Solid line is from *Hellerman and Rosenstein* [1983]. Red is from *Trenberth et al.* [1989]. Note that the ECMWF stresses are much higher in the Southern Ocean. (b) Applied (solid line) and restoring (dashed line) water flux, zonally averaged, for P2. Note that the fluxes are in opposite directions in the Southern Ocean. Since the deep ocean is salty, the implication is that the applied fluxes are making the surface too fresh. When the restoring correction is added to the applied flux (symbols in Figure 4b) the result is a far smaller applied freshwater flux in the Southern Ocean.

inafter referred to as Dunne et al., submitted manuscript, 2004), which links particle export to primary productivity and chlorophyll concentration at 119 sites using

$$\begin{aligned} \mathrm{pe} &= \mathrm{Pe}/\mathrm{PP} \\ &= *\max(0.042, \min(0.72, -0.0078 \times T + 0.0806 \times \ln(\mathrm{Chl}) \\ &\quad + 0.433)), \end{aligned} \tag{1}$$

where pe is pe ratio, Pe is particle export, and PP is primary productivity.

[18] In the work of Dunne et al. (submitted manuscript, 2004) all estimates of primary productivity were made in situ. This paper extends their work by using primary productivity estimates from satellite-based estimates of chlorophyll concentration.

[19] Since significant uncertainties remain about how to estimate primary productivity from ocean color, we use three estimates of this term. The first uses the algorithm of *Behrenfeld and Falkowski* [1997] (hereinafter BF97), which includes an eighth-order polynomial estimate of the temperature-dependent optimal photosynthetic efficiency (P_B^{opt}) with a maximum at around 20°C. The second estimate uses the algorithm of *Carr* [2002], which assumes an exponential temperature dependence for P_B^{opt} similar to that of *Eppley* [1972]. The third estimate uses the primary productivity estimate of *Lee et al.* [1996]. The algorithm for primary production used in this paper is documented by *Marra et al.* [2003]. We use satellite estimates of chlorophyll concentration from SeaWiFS.

[20] Figure 5 shows the estimated zonally integrated particle export using equation (1) for the three separate estimates of primary productivity. The *Carr* [2002] parameterization produces a value of export that is twice that of the BF97 algorithm in the tropics, while the *Marra et al.* [2003] parameterization is higher in the tropics and substantially lower in the subpolar regions.

3. Model Simulations of Biogeochemical Cycling: An Overview

[21] Before examining the differences between the model circulation and tracer budgets, it is worthwhile to examine how well the models simulate a range of biogeochemical fields. From Figure 2 it is clear that model HH simulates the ventilation of the deep ocean much better than LL. Figure 6, which shows the AOU error for HH, P2, and P2A, shows that the latter two models also are able to produce a deep ocean which is sufficiently ventilated. Similar improvements are seen in the radiocarbon distribution within the Pacific (not shown here).

[22] Comparisons between satellite-based and modeled particle export also show significant improvement relative to GSGS due to a revision of the satellite-based estimates. In Figure 7, the four models in Figure 6 are compared with the three observationally based estimates from Figure 5 using SeaWiFS chlorophyll and the three different primary productivity algorithms. Basin-scale integrals are presented in Table 2. The qualitative agreement between models and observational estimates is much better than in GSGS, with all the estimates of particle export showing three latitudinal maxima. By contrast, in GSGS the two estimates of new production had only two latitudinal maxima. The BF97 algorithm produced latitudinal maxima in the high latitudes but none in the tropics, while the *Eppley* [1972] exponential P_B^{opt} eliminated the Southern Ocean maximum.

[23] Using particle export rather than new production changes the regions where the model-data mismatch is the greatest. In GSGS the biggest differences between the models and the observational estimates were in the tropics, while at least one model was consistent with the observa-

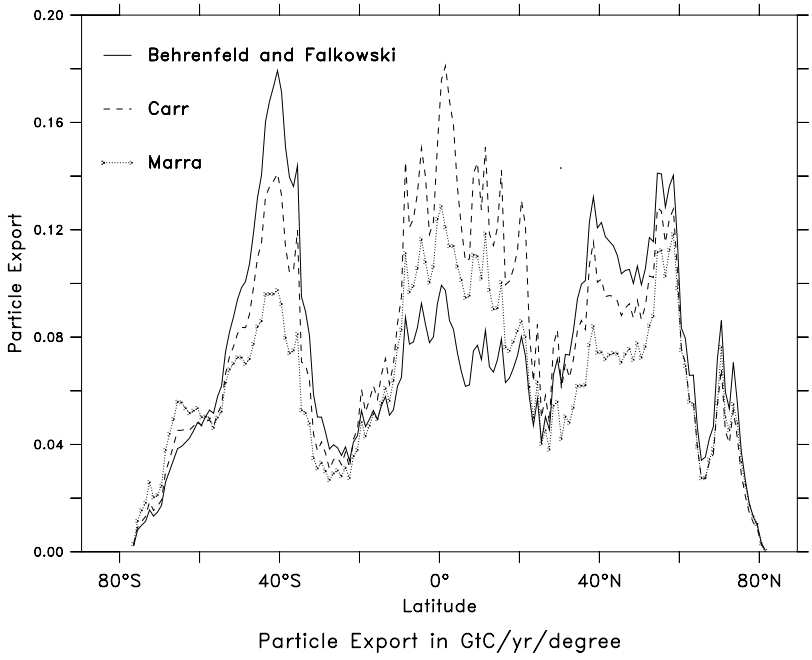

Figure 5. Particle export in GtC/yr/degree using three observational estimates of primary productivity (as outlined in the text) and the regression of Dunne et al. (submitted manuscript, 2004). Note that there are three lobes, in contrast to the result reported in GSGS. This is due both to the use of new observational estimates for chlorophyll (which have more chlorophyll in the tropics) and the new pe-ratio parameterization which allows for higher pe ratios in high-productivity tropical regions.

tional estimates between 50°N and 70°N [*Gnanadesikan et al.*, 2002, Figure 16]. In the current study, the observational range in the tropics (3.2–5.0 GtC/yr) brackets the two models with low vertical mixing (LL and P2A). The model with an intermediate level of mixing (P2) has a tropical particle export of 5.6 Gt/yr, slightly higher than the highest observational estimate (that of *Carr* [2002]). The HH model has a tropical particle export of 7.7 GtC particle export, 50% higher than the highest of the three observational estimates and more than 140% larger than the BF97 observational estimate. The argument made in previous papers that high levels of diapycnal diffusivity are inconsistent with observed tropical productivity given our understanding of particle remineralization [*Gnanadesikan and Toggweiler*, 1999; *Gnanadesikan et al.*, 2002] is supported by the overprediction of particle export by HH. The caveat is important, as increasing the depth at which remineralization occurs has a tendency to lower the rate of biological production. The conclusion that can be drawn from the overprediction of tropical production in HH is thus either that the diffusion coefficient is too high, or that the OCMIP2 scheme produces remineralization that is too shallow. Preliminary high-resolution simulations indicate that both mechanisms may be at work as they tend to produce slightly higher values for tropical particle export (6.0 GtC/yr), even though they have low vertical diffusion in the tropical pycnocline.

[24] In contrast to GSGS, where the biggest area of disagreement was the tropics, the biggest area of disagreement in this study is the Northern Hemisphere. As discussed in GSGS, a major source of disagreement between the models and the observational estimates is the lack of export production in the North Pacific. The North Pacific particle export in the models ranges between 0.29 and 0.62 GtC/yr. This is much smaller than the estimates of particle export from satellite color, which range between 1.3 and 1.8 GtC/yr. This lack of particle export is in large part responsible for the mid-depth AOU errors seen in Figure 6.

[25] The failure of many coarse-resolution models to simulate the temperature, salinity, and nutrient structure of the North Pacific was discussed in detail in GSGS. There it was argued that the boundary conditions applied to the models failed to simulate the formation of a water mass with high preformed nutrients in the northwest Pacific. The dynamics of how this water mass is formed remains a topic of current research, but preliminary results suggest that the problem arises from applying a strong temperature restoring in the presence of boundary currents that separate too far to the north. The outcrop of the $\sigma_\theta = 26.8$ surface occupies a relatively small area in the northwest Pacific, and a Kuroshio that separates from the coast too far from the north (a phenomenon found in models at 1° resolution as well as at 4°) moves large fluxes of tropical water into an area where the surface is being restored toward subpolar conditions. This produces a water mass that is too warm, salty, and nutrient-poor and reduces production throughout the North Pacific. More recent studies using the OCMIP protocol in a model where the fluxes are computed by directly calculating the fluxes using a prescribed atmosphere (which does not have a sharp front in temperature at the northern edge of the

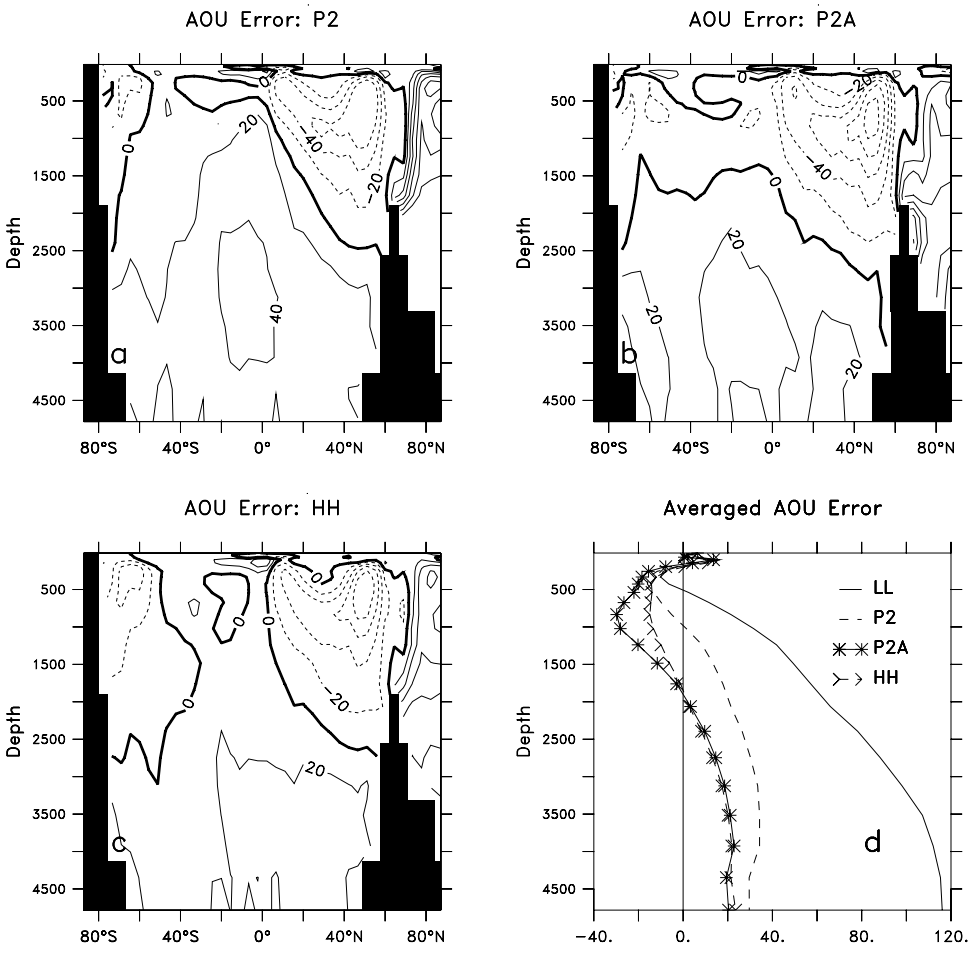

Figure 6. AOU errors (relative to World Ocean Atlas 2001 [*Conkright et al.*, 2002]) from the new models compared with AOU errors in LL. Results demonstrate that the changes to model physics and forcing do improve the ventilation of the deep ocean. Note, however, that all the simulations have too little AOU in the northern subpolar thermocline. (a) P2. (b) P2A. (c) HH. (d) Horizontally averaged AOU error including LL.

Kuroshio and so does not strongly restore the SSTs toward subpolar values) do not show this behavior.

[26] In combination, the new models and observational estimates of particle export result in a significant improvement in model-data mismatch. Figure 8 reproduces Figure 2, but using particle export rather than new production. The data do not lie off the trend line of the models, and models P2 and P2A are quite close to the observations. P2 lies within the error bars for the radiocarbon, CFC-11 inventory, global particle export, and Southern Ocean particle export and is quite close to the observed AOU. P2A also lies within the error bars for radiocarbon, AOU, and tropical particle export, is slightly high for CFC-11 and Southern Ocean particle export, and would lie within the error bars for global particle export given higher export in the North Pacific. In contrast to Figure 2, the revised assessment based on SeaWiFS-based particle export gives no sense that matching both satellite-estimated rates of biological cycling and water mass tracers of ocean ventilation is necessarily inconsistent.

[27] A major contributor to the improvement in the model-data fit is that we use particle export rather than new production. This means that we are comparing our satellite estimates of biological cycling against a smaller value in the models, as the OCMIP models have a significant amount of export associated with dissolved organic matter. Because of the short lifetime (6 months) of this DOM, it rapidly returns to the mixed layer, fueling new production there. Approximately one third of the "new" production in the models is sustained through this DOM cycling.

[28] In order to judge the ability of models to simulate observed patterns, it is helpful to examine multiple patterns simultaneously. *Taylor* [2001] proposed a diagrammatic way of comparing multiple patterns within and across models. The diagram he proposed is a polar plot in which the radius is the ratio of the standard deviation of the model to that of the data, and the angle is the inverse cosine of the correlation. In other words, the radius shows whether the model gets the right amplitude of variability, while the angle

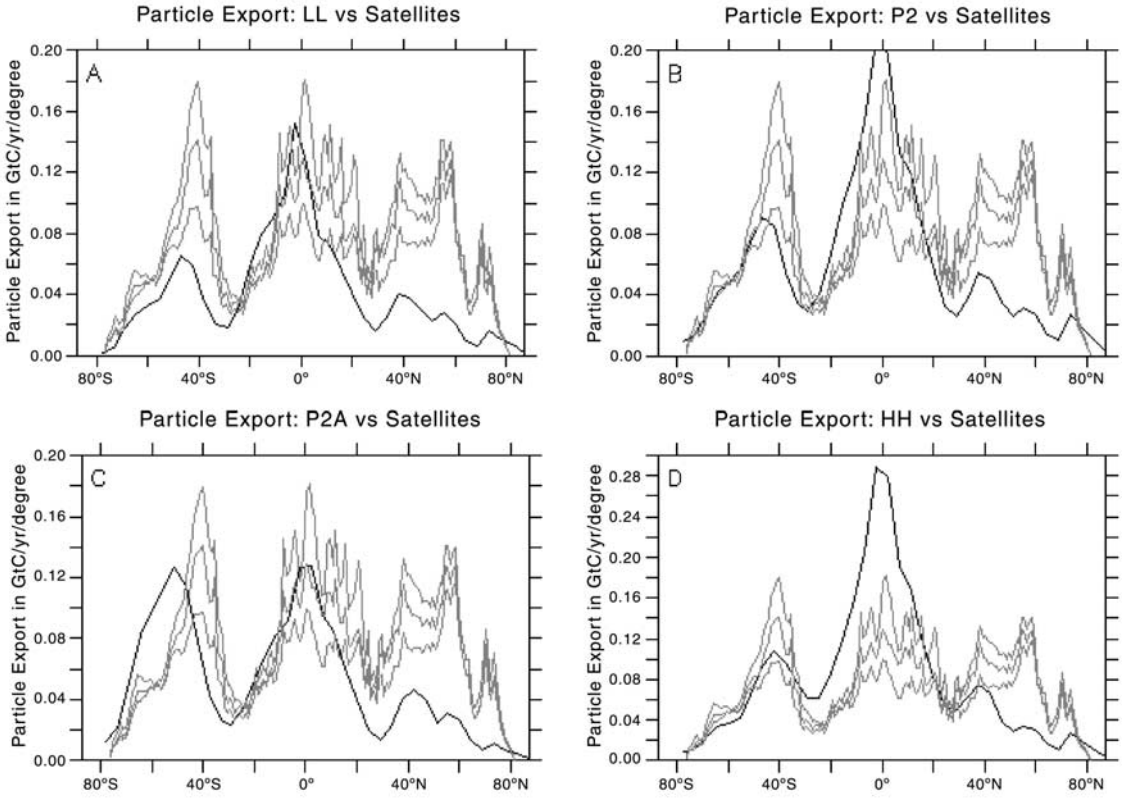

Figure 7. Comparison of observational estimates and models of particle export. Dashed lines are the observational estimates. Solid lines are the models. (a) LL. Note that this model is roughly in the right range in the tropics, but lies below the observational estimates outside the tropics. (b) P2. This model is higher than observations in the tropics, close to the Marra curve in the Southern Ocean, and too low in the north. (c) P2A. Note the displacement of the Southern Ocean export in this simulation. (d) HH. Vertical axis is extended. Note that the tropical production is now severely overestimated. See color version of this figure at back of this issue.

shows whether the variability has the right spatial pattern. The distance from the (1, 0) point on the plot is then the normalized unbiased RMS error.

[29] On a Taylor diagram, different fields will pick out different aspects of the structure of the ocean circulation. For example, temperature is low in the deep and high in the surface. The Taylor diagram essentially provides a measure for whether the location of the vertical temperature gradient is correct. By contrast, oxygen is low in mid-depth waters, so the Taylor diagram for oxygen is much more sensitive to the ventilation of these water masses. Radiocarbon has a large contrast between the Atlantic and Pacific Ocean, so the Taylor diagram for radiocarbon will weight small differences in ventilation between these ocean basins much more heavily than the Taylor diagram for temperature.

[30] A composite Taylor diagram, showing comparisons between T, S, radiocarbon, AOU, phosphate, and the monthly varying, zonally averaged particle export is shown in Figure 9. A zonal average was used to eliminate spurious low correlations arising from extreme values of particle

Table 2. Particle Export in GtC/yr From Different Regions Using Three Different Observational Estimates of Export and the Four General Circulation Models Described in the Text[a]

Estimate/Region	Global	Northern Pacific (>30°N)	Northern Atlantic (30°N–75°N)	Tropics (23°S–23°N)	Southern Ocean (<30°S)
Behrenfeld Falkowski	11.1	1.8	1.7	3.2	3.4
Carr	12.0	1.6	1.4	5.0	2.9
Marra	9.7	1.3	1.2	3.9	2.4
PRINCE1	6.9	0.31	0.64	**3.9**	1.6
PRINCE2	**10.0**	0.39	0.85	5.6	**2.4**
PRINCE2A	8.8	0.29	0.79	**3.7**	**3.5**
HIMIX	13.0	0.62	0.95	7.7	**2.7**

[a]Model results which lie within the range of the observational estimates are highlighted in bold.

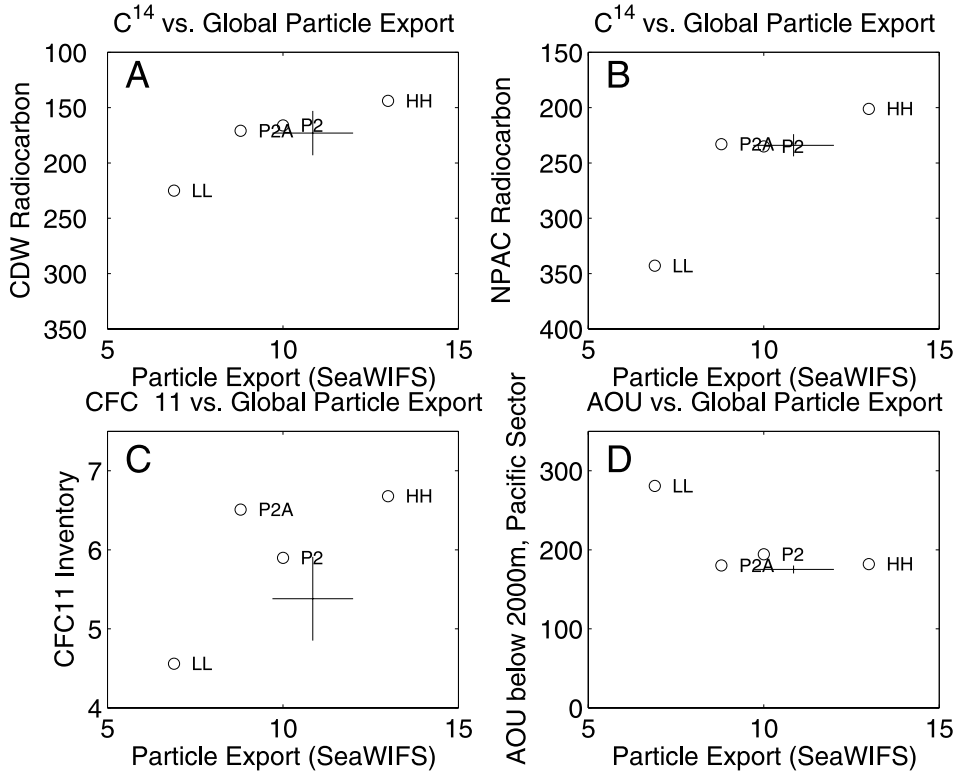

Figure 8. Particle export versus water mass tracers for the LL, HH, P2, and P2A. (a) Particle export versus radiocarbon in Circumpolar Deep Water. (b) Particle export versus radiocarbon in the North Pacific. (c) Particle export versus global CFC-11 inventory ($\times 10^8$ mol). (d) Particle export versus deep AOU in the Pacific sector. Note that the P2 model is close to the data in all four plots. P2A is close, with somewhat better AOU, lower particle export, and higher CFC-11 inventory.

export in coastal points not resolved by the model. The results show that the spatiotemporal distribution of particle export remains much more poorly simulated than any of the hydrographic parameters. At their best, the models explain 40% of the observed zonally averaged spatiotemporal variance of export flux, substantially better than the upper limit of 20% found in GSGS but still far below the model performance for radiocarbon or even oxygen. The correlations are substantially better for the *Carr* [2002] and *Marra et al.* [2003] parameterizations than they are for the BF97 parameterization, consistent with our earlier results. Some of this improvement stems from the use of the SeaWiFS chlorophyll data set, which has higher retrievals in the tropics, particularly the Pacific [*Gregg et al.*, 2002], so that parameterizations of production such as BF97 are able to produce a local maximum there. Additionally, the Dunne et al. (submitted manuscript, 2004) representation of pe ratio allows for higher export in the tropics since it allows for higher pe ratios when the production is high, even at high temperatures. The results also show that although the distribution of oxygen and radiocarbon are significantly improved in the P2 and P2A models relative to LL, the new models do not capture a higher fraction of the variability in the particle export. By contrast, the distributions of temperature and salinity (the best-known hydrographic fields) are best simulated in LL, so that there is no model that unambiguously produces a "best" solution for all fields. Given this fact, it is worth examining how the different models arrive at different solutions.

4. What Mechanisms Maintain an Adequately Ventilated Deep Ocean With Respect to Oxygen and Radiocarbon?

[31] We have shown that our new models come closer than LL to reproducing both estimates of the rate of biological cycling, the impact of that cycling on the AOU field, and the distribution of radiocarbon within the deep ocean. The first improvement is largely driven by changes in the data, and the latter two by changes in the models. In this section we focus on understanding the changes in the models. In particular, we seek to understand what it is about the high-mixing models that produces increased ventilation, and to what extent these processes are replicated in the low-mixing models with altered Southern Ocean boundary conditions.

[32] We begin by looking at the budget for oxygen and radiocarbon in the North Pacific, where some of the largest errors were found in the LL model. Figure 10 shows budgets of oxygen and radiocarbon between 25°N and 60°N and 120°E and 105°W in the North Pacific. The column is divided into three boxes, from the surface to 1365 m (model level 14), from 1365 to 4131 m (bottom of model level 21)

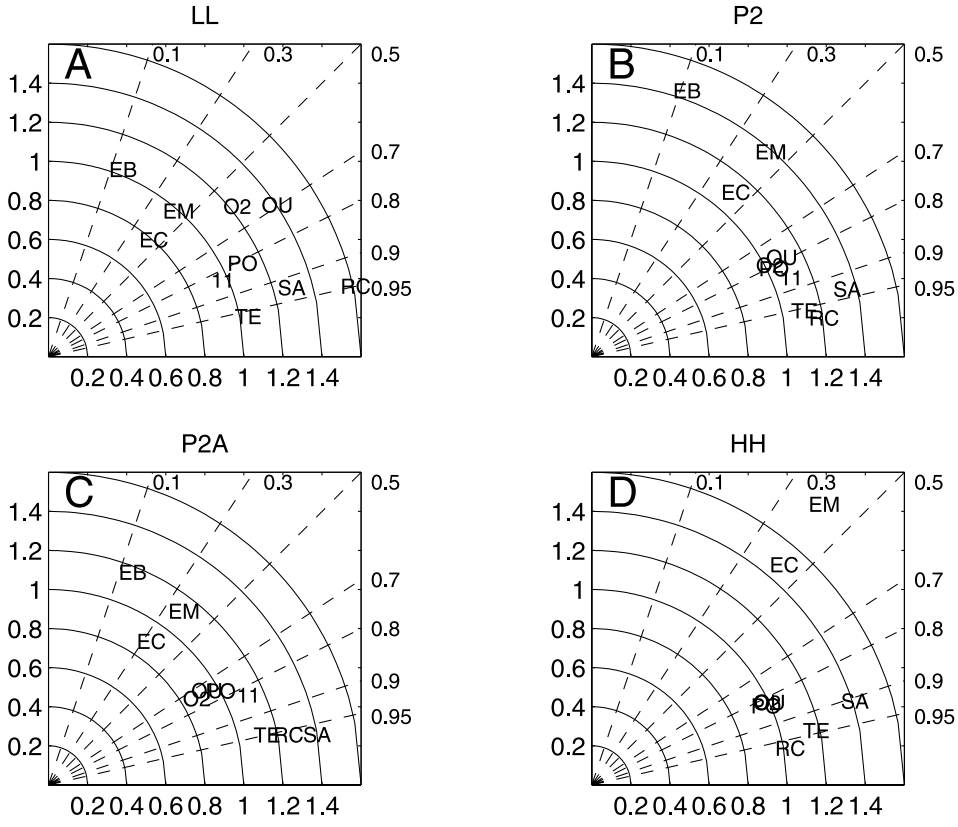

Figure 9. Taylor diagrams including particle export for four of the models. TE is temperature, SA is salinity, O2 is oxygen, OU is apparent oxygen utilization, PO is phosphate, RC is radiocarbon, 11 is CFC-11, EB is export production using BF97, EC is export production using work of *Carr* [2002], and EM is export production using work of *Marra et al.* [2003]. Export production is the monthly-varying zonal average. All other fields are the three-dimensional annual average. The results show graphically that although the newer models produce a tighter clustering of the hydrographic parameters, they do not produce a tighter clustering of the export production. (a) LL. (b) P2 (c) P2A. (d) HH (EB is off the chart for this model).

and from 4131 to 5000 m. Advective fluxes (in black) are distinguished from diffusive fluxes (in red). A number of interesting conclusions can be drawn from this figure.

[33] 1. Both advection and diffusion play first-order roles in determining the supply of oxygen and radiocarbon to the deep North Pacific in the GCMs. For example, in the bottom box in model LL (top row), advection accounts for two thirds of the oxygen supply and slightly less than one half of the radiocarbon supply. Neither advection nor diffusion can be neglected in the budget.

[34] 2. Both lateral and vertical processes can play an important role in the budget. Examination of the different models shows cases where vertical processes dominate the supply (as for oxygen and radiocarbon in P2A) or horizontal processes dominate the supply (as in HH and P2).

[35] 3. Model HH increases the oxygen while also increasing the oxygen demand. It solves the problem of supplying more oxygen to the North Pacific by increasing the advective flux below 1365 m (from 1.33 Tmol/yr to 3.99 Tmol/yr) and by increasing the lateral diffusive flux (from 1.17 Tmol/yr to 3.91 Tmol/yr). This is partially compensated by a switch in the direction of the vertical advective flux, representing entrainment of intermediate waters into North Pacific Deep Waters.

[36] 4. Model P2 solves the problem of supplying more oxygen to the deep North Pacific primarily by increasing the lateral advective flux. The vertical diffusive flux in this model actually switches sign, as oxygen is diffused into the oxygen minimum zones near the equator.

[37] 5. Model P2A solves the problem of supplying more oxygen to the deep North Pacific by increasing the vertical advective flux. In sharp contrast to P2 and P2A, the deep lateral advective and diffusive fluxes in this model essentially sum up to zero.

[38] 6. Diffusion plays a much bigger role for radiocarbon than it does for oxygen. For example, diffusive fluxes account for 69% of the supply of radiocarbon below 1365 m in LL, 81% in HH, 66% in P2, and 41% in P2A. The comparable numbers for oxygen are 35%, 48%, 11%, and −45% (diffusion actually acts as a sink in the latter case). Lateral diffusion is about twice as important as vertical diffusion for supplying radiocarbon in all of the model runs.

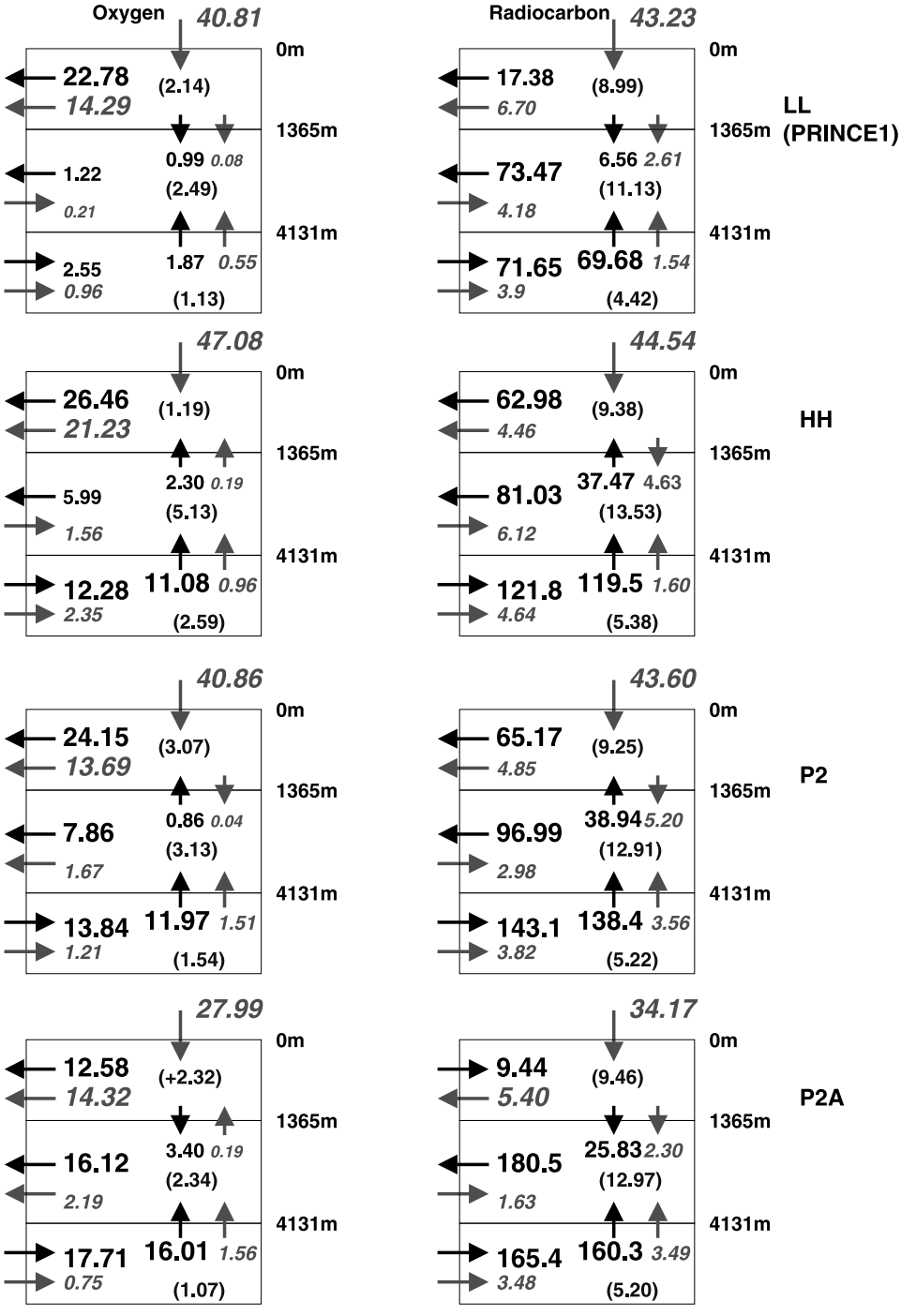

Figure 10. Budgets of oxygen (in Tmol/yr) and radiocarbon (in mol/yr) in the North Pacific (north of 25°N) in four models. Advective fluxes are in black, diffusive are in red, and consumption terms are in blue. See color version of this figure at back of this issue.

[39] 7. The advective fluxes of oxygen and radiocarbon are far larger in HH, P2, and P2A than in LL. This is both because the deep concentrations increase and because the magnitude of the flows increase.

[40] A similar plot can be made for the Southern Ocean (Figure 11). The differences between models in this plot reinforce the conclusions from Figure 10. Especially with respect to radiocarbon, the HH model has a completely different advective pattern than the other models, with a net flux out of the tropics, downward advection of radiocarbon in the Southern Ocean, and deep advective export of radiocarbon. The oxygen flux in the HH model is also strikingly different, with net downward advection and deep export of oxygen. The lateral diffusive fluxes are significant in all of the models. The lateral diffusive flux of radiocarbon is of the same order as the net advective flux, sometimes

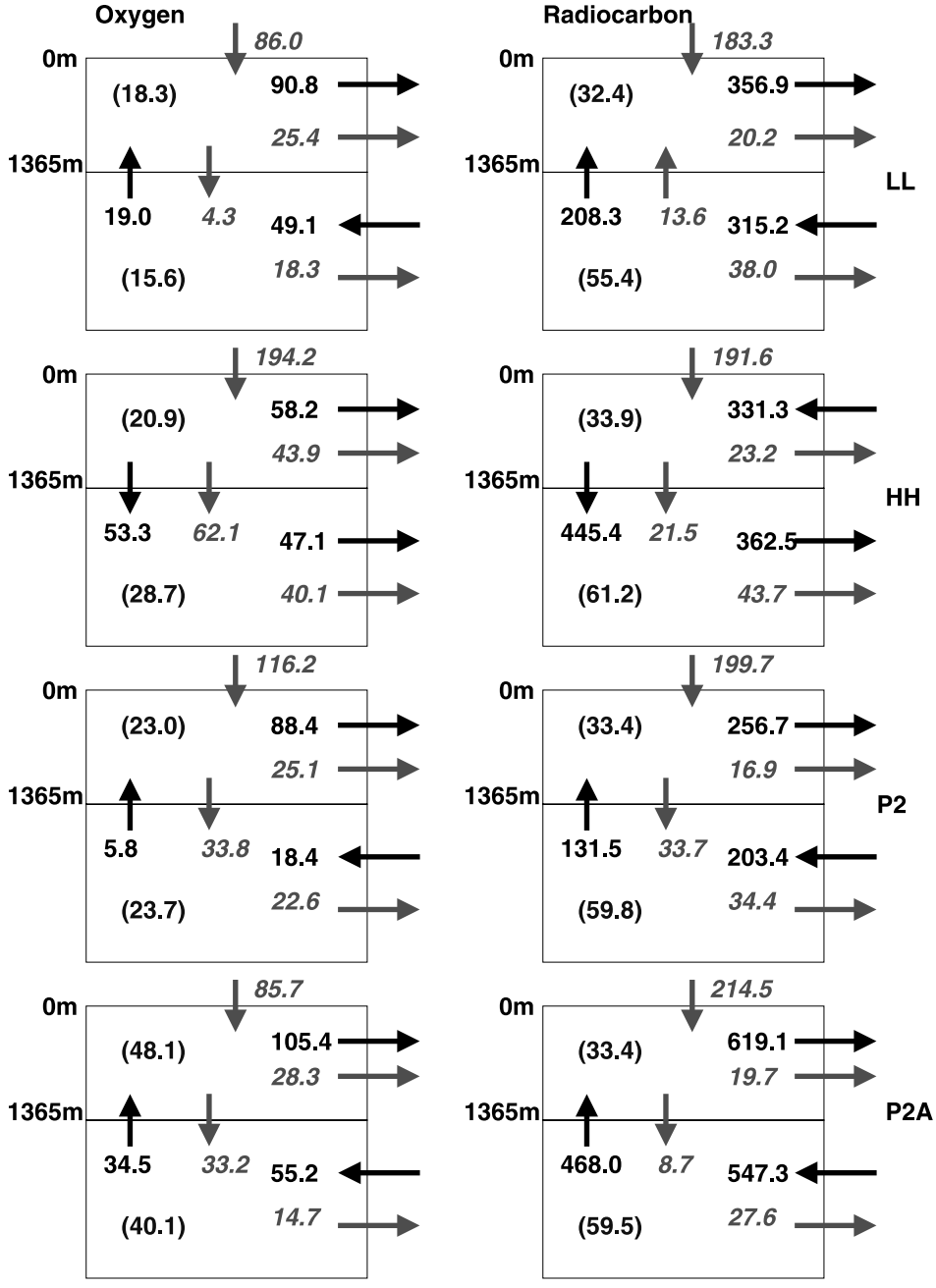

Figure 11. Budgets of oxygen (in Tmol/yr) and radiocarbon (in mol/yr) within the Southern Ocean in four models. See color version of this figure at back of this issue.

larger and sometimes smaller. The net inflow of oxygen and radiocarbon in P2A, which has higher Southern Ocean winds, is significantly larger than in the other models.

[41] A particularly surprising result from Figure 11 is the upward diffusive flux of radiocarbon in model LL. In order to understand how such a flux is possible, one must remember that the vertical diffusive term in this model includes not only the small-scale diffusion, but all mixing terms, including those associated with the isopycnal mixing of thickness: the GM terms. The GM terms act to flatten isopycnals, resulting in a net upwelling (of lighter, younger waters) in lower latitudes and downwelling (of denser, older waters) in high latitudes. In the LL case this term overwhelms all the other vertical diffusive terms within the Southern Ocean.

[42] The changes in the advective supply of radiocarbon and oxygen resulting from differences in mixing can be readily explained in terms of the different pathways of vertical exchange in the model. Figure 12a shows the northward transport of water with a density lighter than 27.4 in the original model suite. An increase means that dense water is being converted to light water, while a decrease means that light water is being converted to dense water. In the models with high vertical mixing, the northward transport increases throughout the tropics, implying that

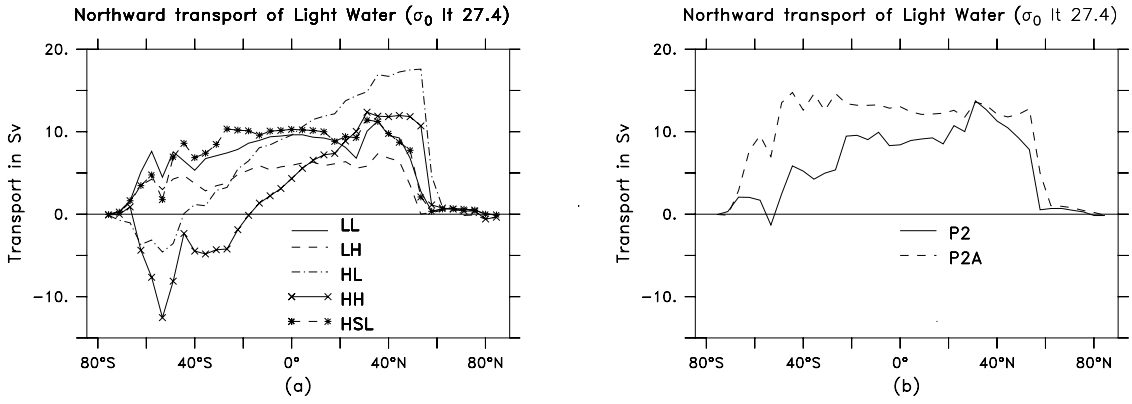

Figure 12. Northward transport of water with σ_θ less than 27.4. Increasing values to the right mean that dense water is being converted to light water. Decreasing values to the right mean that light water is being converted to dense water. (a) Models LL (black), LH (red), HL (green), HH (dark blue), and HSL (light blue). Note that the models with high pycnocline mixing (HH and HL) slope upward to the right across the tropics, indicating that dense water is being converted to light water there. Note also the relatively small difference between HSL and LL. (b) Models P2 and P2A. Note that model P2 is intermediate between LL and HH, having some slope in the tropics. Model P2A has virtually none as the stronger Southern Ocean winds drive a more uniform northward transport. See color version of this figure at back of this issue.

deep water is upwelling and being converted to light water. In the models with low vertical mixing, by contrast, much more of the light water is converted to dense water in the Southern Ocean [*Gnanadesikan et al.*, 2003]. Figure 12b shows the equivalent plot for P2 and P2A. Model P2 has slightly more upwelling in the tropics than LL, but only slightly. Model P2A has a much larger Southern Ocean upwelling, as would be expected from the much higher Southern Ocean winds associated with the ECMWF wind product.

[43] The results in Figures 10 and 11 suggest that the impact of changing one parameter within a general circulation can be quite complicated. We can see this in more detail in Figure 13, which shows zonally integrated changes in the global radiocarbon budget associated with increasing vertical diffusion (HL-LL), lateral diffusion (HH-HL), and Southern Ocean diffusion (HSL-LL).

[44] Increasing the vertical diffusion coefficient (Figure 13a) results in a complex pattern of changes in the fluxes. The large-scale pattern of change in the advective flux is exactly as might be expected from comparing the HL and LL lines in Figure 12a. The high-mixing water has much more transformation of dense to light water within the tropics, implying more upwelling there. This results in a substantial increase in the air-sea flux there and an increase in the flux of younger waters to the Southern Ocean and high-latitude northern ocean surface boxes. In these boxes, however, vertical diffusion takes over, moving the additional radiocarbon down into the water column. At depth, the advective flux then moves this additional radiocarbon into the tropics, where some of it diffuses back into the high latitudes and some is lost through decay.

[45] By contrast, increasing the lateral diffusive coefficient (Figures 12a and 13b) tends to counter the interhemispheric overturning circulation, reducing the flow of surface water from the Southern Ocean into the tropics and from the tropics to the North Atlantic. This actually results in an increase in the advective surface divergence in the tropics and a slight decrease in radiocarbon concentration (as indicated by the smaller decay term). The slowdown in the export of Southern Ocean surface waters allows them to increase their radiocarbon concentration (they are not being exported to the north as rapidly). In the deep ocean, the larger diffusive coefficient removes radiocarbon from the Southern Ocean. As a result the vertical gradient of radiocarbon increases, and the vertical diffusive flux increases slightly. Overall, however, there is a very slight decrease in the uptake of radiocarbon, and the ocean grows slightly older, as the slowdown in the vertical advective flux is not quite compensated by the increase in vertical diffusive flux.

[46] Increasing the vertical diffusion coefficient within the Southern Ocean alone produces a change in the budgets of radiocarbon that is completely unlike the patterns resulting from changing either the vertical or lateral diffusion coefficients globally. The main effect of increasing the vertical diffusion coefficient within the Southern Ocean is to increase the ventilation of intermediate waters, substantially increasing the radiocarbon values in these waters (examination of the tracer fields shows an increase of 30 per mil). This additional radiocarbon is advected northward in the interhemispheric overturning. Some of it sinks to join the North Pacific Deep Water in the Pacific, resulting in a significant increase in radiocarbon consumption in the deep ocean. Some fraction of this radiocarbon then diffuses back toward high latitudes in the deep ocean.

[47] The differences in circulation are strongly reflected in the surface distribution of radiocarbon. Figure 14 shows the surface radiocarbon concentration in all seven models compared with data, assuming 2000 as a nominal comparison year (done so as not to have to worry about the separation between natural and bomb radiocarbon). The high-mixing models have surface radiocarbon concentrations that are systematically too low, a result consistent with the earlier work of *Toggweiler and Samuels* [1993]. The lower mixing results give a better match to the

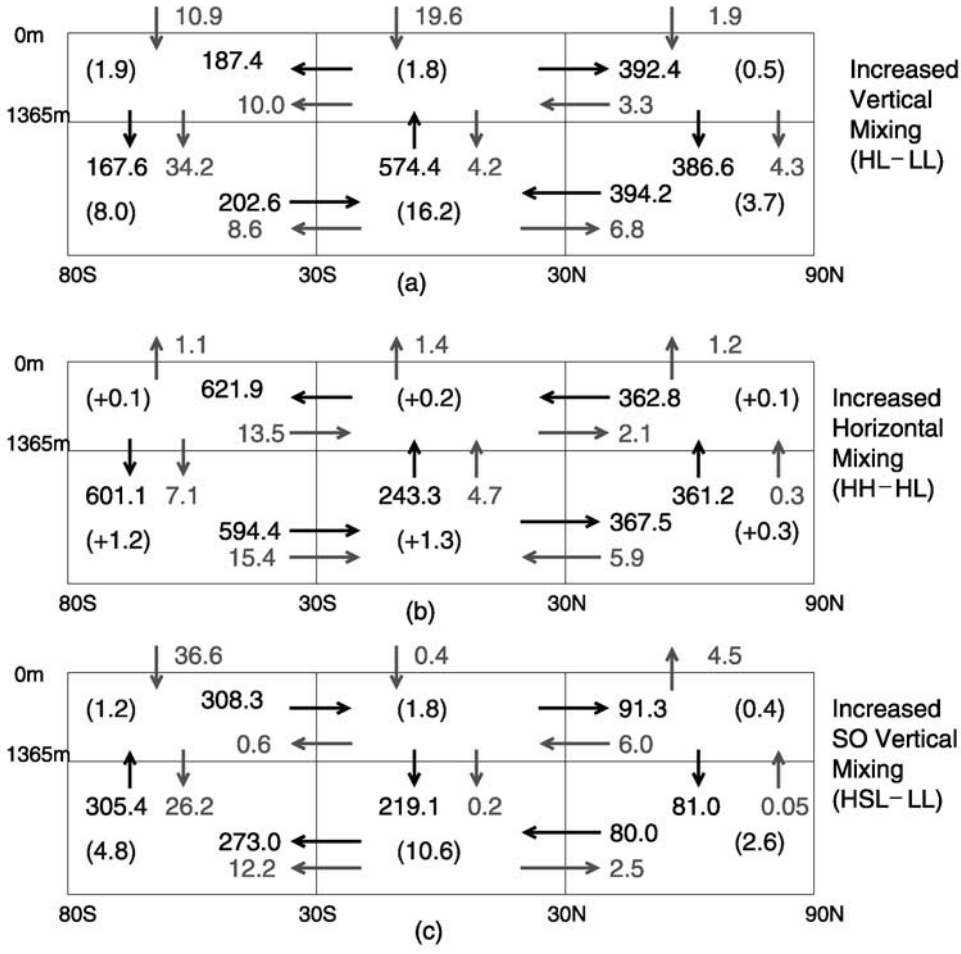

Figure 13. Sensitivity of zonally averaged radiocarbon budget to different parameterizations of mixing (in mol/yr). Note that as before, certain regions are out of balance due to decadal transients. (a) Increase in the vertical mixing (difference between HL and LL). (b) Increase in the lateral mixing (difference between HH and HL). (c) Increase in vertical mixing within the Southern Ocean only (difference between HSL and LL). See color version of this figure at back of this issue.

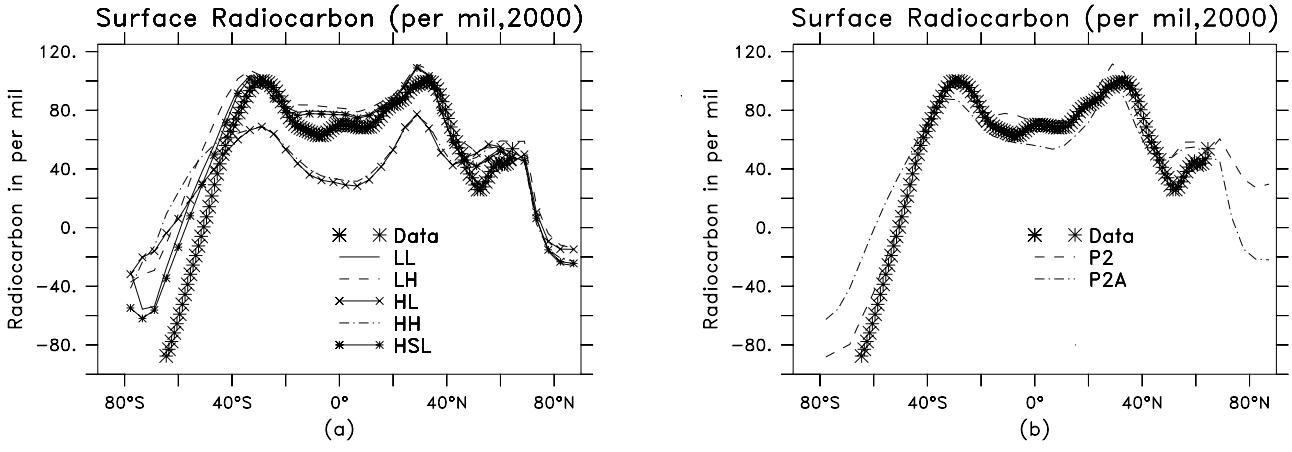

Figure 14. Zonally averaged surface radiocarbon values for models (lines) and data (stars). (a) GSGS model suite. (b) Models P2 and P2A. Note that P2 does the best job at reproducing surface values (which include a bomb component). See color version of this figure at back of this issue.

observed surface values. The best solution is found for the P2 model.

5. Conclusions

[48] A major question we asked at the beginning of this paper regarded the extent to which measurements of global biogeochemical cycling can be used to learn about the details of vertical exchange. While such approaches are common among geochemists (see *Broecker et al.* [1999] and *Orsi et al.* [2002] for a recent exchange), the use of tracers to infer the pathways of exchange has been criticized. For example, *Wunsch* [2002] has argued that tracers actually add relatively little information about the dynamics of the large-scale flow because their boundary conditions are poorly known. While this paper supports the utility of tracers for understanding the ocean circulation, it also places some caveats on their use. While biogeochemical cycling estimates are clear markers about when the circulation is getting something wrong (as in model LL, which has far too little ventilation of the deep ocean), they do not provide an unambiguous picture of how such problems may be fixed. For example, models may produce better ventilation of the deep Southern Ocean either by increasing the amount of vertical mixing (as in HH and P2), increasing the supply of younger waters from the tropics (as in HH, but not P2 or P2A), or increasing the net inflow of waters from the Atlantic (as in P2A). While we would strongly suggest that the overprediction of tropical particle export and the underprediction of surface radiocarbon mitigate against a choice of high vertical diffusion coefficients, the results are not unambiguous, since lower errors near the surface may be balanced by higher errors at depth. In addition, a good simulation of radiocarbon (in the sense of minimizing errors on the global scale) does not result in an unambiguous determination of the direction of certain important fluxes, let alone their magnitude.

[49] The complexity of the flow, and the fact that the response to changes in parameters such as diffusion coefficients is not straightforward, underlines both the utility of general circulation models for understanding tracer distributions and the difficulty in verifying such models with data. Because the indirect effects of changing parameter settings can dwarf the direct effects, it is impossible to understand the sensitivity of tracer distributions to mixing processes without running a full model. While the large-scale pattern of the impact of diffusive coefficients on advective fluxes can be qualitatively understood using the simple theory of *Gnanadesikan* [1999a], the theory does not capture how the flux of radiocarbon can be "handed off" between advection and diffusion. Given that the flux divergences may be relatively small in comparison to gross advective fluxes of oxygen and radiocarbon, it may prove difficult to close the budget from observations alone.

[50] A particularly important result of this work is that lateral diffusion plays a major role in determining the budgets of radiocarbon and oxygen. This is significant because lateral diffusive terms are particularly poorly constrained by direct measurements. Many box models (such as the widely used PANDORA model) effectively neglect such terms. Observing lateral diffusion requires capturing correlations between biogeochemical tracers and velocity on the spatial scale of ocean eddies (10–30 km in midlatitudes). It is far from clear that this can be done observationally. A better understanding of the diffusive effects of realistic eddies throughout the global ocean would appear to be necessary in order to close budgets of important tracers.

[51] **Acknowledgments.** This work was supported by the Department of Energy Office of Biological and Environmental Research under the Ocean Carbon Sequestration Initiative (DOE grant DE-FG0200ER63009), the Carbon Modeling Consortium (NOAA grant NA56GP0439), and the NOAA Geophysical Fluid Dynamics Laboratory. R. M. Key was supported under NOAA grants NA96GP0200 and NSF grants OCE-9986310. We thank Joellen Russell, Bryan Arbic, and two anonymous reviewers for useful suggestions on an earlier draft of this paper and the SeaWiFS project (code 970.2) and Goddard Earth Sciences Data and Information Services Center/Distributed Active Archive (code 902) at the Goddard Space Flight Center, Greenbelt, Maryland, for the production and distribution of these data, respectively. These activities are sponsored by NASA's Earth Science Enterprise.

References

Behrenfeld, M. J., and P. G. Falkowski (1997), Photosynthetic rates derived from satellite-based chlorophyll concentration, *Limnol. Oceanogr.*, *42*, 1–20.

Broecker, W. S., S. Sutherland, and T. H. Peng (1999), A possible slowdown of Southern Ocean deep water formation, *Science*, *286*, 1132–1135.

Carr, M. E. (2002), Estimation of potential productivity in Eastern Boundary Currents using remote sensing, *Deep Sea Res., Part II*, *49*, 59–80.

Conkright, M., R. A. Locarnini, H. E. Garcia, T. D. O'Brien, T. P. Boyer, C. Stephens, and J. I. Antonov (2002), World Ocean Atlas 2001: Objective analysis, data statistics and figure (CD-ROM documentation), report, 17 pp., Natl. Oceanogr. Data Cent., Silver Spring, Md.

Da Silva, A., A. C. Young, and S. Levitus (1994), *Atlas of Surface Marine Data 1994*, vol. 1, *Algorithms and Procedures*, *NOAA Atlas NESDIS 6*, Natl. Oceanic and Atmos. Admin., Silver Spring, Md.

Dixon, K. W., J. L. Bullister, R. H. Gammon, and R. J. Stouffer (1996), Examining a coupled climate model using CFC-11 as an ocean tracer, *Geophys. Res. Lett.*, *23*(15), 1957–1960.

Doney, S. C., et al. (2004), Evaluating global ocean carbon models: The importance of realistic physics, *Global Biogeochem. Cycles*, *18*, GB3017, doi:10.1029/2003GB002150.

Dutay, J.-C., et al. (2002), Evaluation of ocean model ventilation with CFC-22: Comparison of 13 global ocean models, *Ocean Modell.*, *4*, 89–120.

England, M. H. (1995), Using chlorofluorocarbons to assess ocean climate models, *Geophys. Res. Lett.*, *22*(22), 3051–3054.

Eppley, R. W. (1972), Temperature and phytoplankton growth in the sea, *Fish. Bull.*, *70*, 1063–1085.

Fahrbach, E., R. G. Peterson, G. Rohardt, P. Schlosser, and R. Bayer (1994), Suppression of bottom water formation in the Southeastern Weddell Sea, *Deep Sea Res., Part I*, *41*, 389–411.

Foster, T. D., and E. C. Carmack (1976), Frontal zone mixing and Antarctic Bottom Water formation in the Southern Weddell Sea, *Deep Sea Res.*, *23*, 301–317.

Gent, P., and J. C. McWilliams (1990), Isopycnal mixing in ocean circulation models, *J. Phys. Oceanogr.*, *20*, 150–155.

Gnanadesikan, A. (1999a), A simple model for the structure of the oceanic pycnocline, *Science*, *283*, 2077–2079.

Gnanadesikan, A. (1999b), A global model of silicon cycling: Sensitivity to eddy parameterization and dissolution, *Global Biogeochem. Cycles*, *13*, 199–220.

Gnanadesikan, A., and J. R. Toggweiler (1999), Constraints placed by silicon cycling on vertical exchange in general circulation models, *Geophys. Res. Lett.*, *26*, 1865–1868.

Gnanadesikan, A., R. D. Slater, N. Gruber, and J. L. Sarmiento (2002), Oceanic vertical exchange and new production: A comparison between models and observations, *Deep Sea Res., Part II*, *49*, 363–401.

Gnanadesikan, A., R. D. Slater, and B. L. Samuels (2003), Sensitivity of ocean heat transport to subgridscale parameterizations in coarse-resolution ocean models, *Geophys. Res. Lett.*, *30*(18), 1967, doi:10.1029/2003GL018036.

Gregg, W. W., M. E. Conkright, J. E. O'Reilly, F. S. Patt, M. H. H. Wang, J. A. Yoder, and N. W. Casey (2002), NOAA-NASA coastal zone color scanner reanalysis effort, *Appl. Opt.*, *41*, 1615–1628.

Griffies, S. M., A. Gnanadesikan, R. C. Pacanowski, V. D. Larichev, J. K. Dukowicz, and R. D. Smith (1998), Isoneutral diffusion in a z-coordinate ocean model, *J. Phys. Oceanogr.*, *28*, 805–830.

Griffies, S. M., R. C. Pacanowski, and R. W. Hallberg (2000), Spurious diapycnal mixing associated with advection in a z-coordinate ocean model, *Mon. Weather Rev.*, *128*, 538–564.

Hellerman, S., and M. Rosenstein (1983), Normal monthly wind stress over the World Ocean with error estimates, *J. Phys. Oceanogr.*, *13*, 1093–1104.

Klinger, B. A., S. Drijfhout, J. Marotzke, and J. R. Scott (2003), Sensitivity of basinwide meridional overturning to diapycnal diffusion and remote wind forcing in an idealized Atlantic-Southern Ocean geometry, *J. Phys. Oceanogr.*, *33*, 249–266.

Laws, E. A., P. G. Falkowski, W. O. Smith, H. Ducklow, and J. J. McCarthy (2000), Temperature effects on export production in the open ocean, *Global Biogeochem. Cycles*, *14*, 1231–1246.

Ledwell, J., A. Watson, and C. S. Law (1993), Evidence for slow mixing across the pycnocline from an open-ocean tracer release experiment, *Nature*, *364*, 701–703.

Lee, Z. P., K. L. Carder, J. Marra, R. G. Steward, and M. J. Perry (1996), Estimating primary production at depth from remote sensing, *Appl. Opt.*, *35*, 463–474.

Levitus, S., R. Burgett, and T. P. Boyer (1994), *World Ocean Atlas 1994*, vol. 3, *Salinity*, *NOAA Atlas NESDIS 3*, 99 pp., Natl. Oceanic and Atmos. Admin., Silver Spring, Md.

Maier-Reimer, E. (1993), Geochemical cycles in an ocean general circulation model: Preindustrial distributions, *Global Biogeochem. Cycles*, *7*, 643–667.

Marra, J., C. Ho, and C. Trees (2003), An alternative algorithm for the calculation of primary productivity from remote sensing data, *Tech. Rep. LDEO-2003-1*, Lamont-Doherty Earth Observatory, Palisades, N. Y.

Matsumoto, K., et al. (2004), Evaluation of ocean carbon cycle models with data-based metrics, *Geophys. Res. Lett.*, *31*, L07303, doi:10.1029/2003GL018970.

Najjar, R. G., J. L. Sarmiento, and J. R. Toggweiler (1992), Downward transport and the fate of organic matter in the ocean: Simulations with a general circulation model, *Global Biogeochem. Cycles*, *6*, 45–76.

Orsi, A. H., W. M. Smethie, and J. L. Bullister (2002), On the total input of Antarctic waters to the deep ocean: A preliminary estimate from chlorofluorocarbon measurements, *J. Geophys. Res.*, *107*(C8), 3122, doi:10.1029/2001JC000976.

Pacanowski, R. C., and S. M. Griffies (1999), *The MOM3 Manual, Alpha Version*, 580 pp., NOAA Geophys. Fluid Dyn. Lab., Princeton, N. J.

Polzin, K. L. (1999), A rough recipe for the energy balance of quasi-steady internal lee waves, in *Aha Hulikoa: Dynamics of Oceanic Internal Gravity Waves II*, pp. 117–128, Univ. of Hawaii at Manoa, Honolulu.

Taylor, K. E. (2001), Summarizing multiple aspects of model performance in a single diagram, *J. Geophys. Res.*, *106*(D7), 7183–7192.

Toggweiler, J. R., and B. Samuels (1993), New radiocarbon constraints on the upwelling of abyssal water to the ocean's surface, in *The Global Carbon Cycle*, pp. 333–366, Springer-Verlag, New York.

Toggweiler, J. R., K. Dixon, and K. Bryan (1989), Simulations of radiocarbon in a coarse-resolution world ocean model 1: Steady state prebomb distributions, *J. Geophys. Res.*, *94*(C6), 8217–8242.

Trenberth, K. E., J. Olson, and W. Large (1989), A global ocean wind stress climatology based on ECMWF Analyses, *Tech. Rep. NCAR/TN-338+STR*, Natl. Cent. for Atmos. Res., Boulder, Colo.

Veronis, G. (1975), The role of models in tracer studies, in *Numerical Models of Ocean Circulation*, pp. 133–165, Natl. Acad. of Sci., Washington, D. C.

Watson, A., et al. (2003), Carbon dioxide fluxes in the global ocean, in *Ocean Biogeochemistry: The Role of the Ocean Carbon Cycle in Climate Change*, edited by M. J. R. Fasham, pp. 123–144, Springer-Verlag, New York.

Willey, D. A., R. A. Fine, R. E. Sonnerup, J. L. Bullister, W. M. Smethie Jr., and M. J. Warner (2004), Global oceanic chlorofluorocarbon inventory, *Geophys. Res. Lett.*, *31*(1), L01303, doi:10.1029/2003GL018816.

Wunsch, C. (2002), Oceanic age and transient tracers: Analytical and numerical solutions, *J. Geophys. Res.*, *107*(C6), 3048, doi:10.1029/2001JC000797.

J. P. Dunne and A. Gnanadesikan, NOAA/Geophysical Fluid Dynamics Lab, PO Box 308, Princeton, NJ 08542-0308, USA. (john.dunne@noaa.gov; gnana@splash.princeton.edu)

R. M. Key, J. L. Sarmiento, and R. D. Slater, Atmospheric and Oceanic Sciences Program, Princeton University, PO Box CN710, Princeton, NJ 08540-071, USA. (key@princeton.edu; jls@splash.princeton.edu; rdslater@splash.princeton.edu)

K. Matsumoto, Agency of Industrial Science and Technology, Site 7, Geological Survey of Japan, 1-1-1 Higashi, Tsukuba, Ibaraki 305-8567, Japan. (katsumi@ni.aist.go.jp)

P. S. Swathi, CSIR Centre for Mathematical Modeling and Computer Simulation, National Aerospace Laboratory, Belur Campus, Bangalore 560 037, India. (swathi@cmmacs.ernet.in)

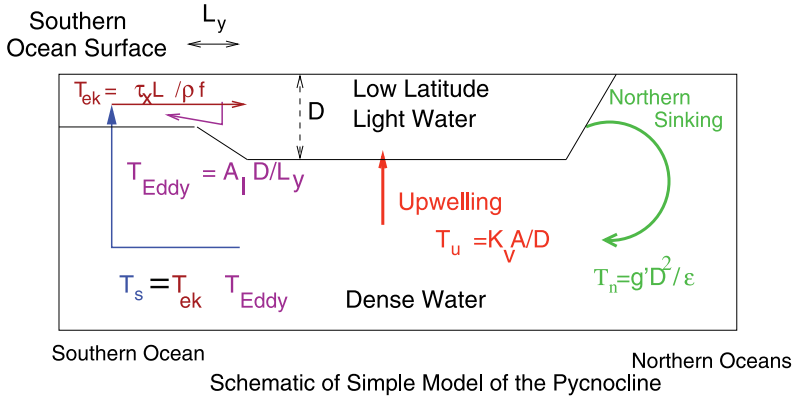

Figure 3. Schematic of the simple model of thermohaline overturning of *Gnanadesikan* [1999a]. Figure is taken from *Gnanadesikan et al.* [2003]. The figure shows four fluxes. The formation of North Atlantic Deep Water is represented by a Northern Hemisphere overturning flux T_n which goes as $g'D^2/\varepsilon$ where g' is the reduced gravity between light and dense water spheres, D is the depth of the pycnocline, and ε is a frictional resistance. This flux may be balanced either by an upwelling flux in tropical latitudes $T_u = K_v A/D$ (where K_v is the diapycnal diffusion coefficient and A is the area of the tropics) or by a Southern Ocean upwelling flux. The Southern Ocean flux is the difference between the Ekman flux $T_{ek} = \tau_x L_x/\rho f$ (where τ_x is the wind stress, L_x is the length of a latitude circle in the Southern Ocean, ρ is density and f is a scale value for the Coriolis parameter) and an eddy flux $T_{eddy} = A_I D/L_y$ (where A_I is a lateral diffusion coefficient and L_y is the scale over which the pycnocline shallows in the south).

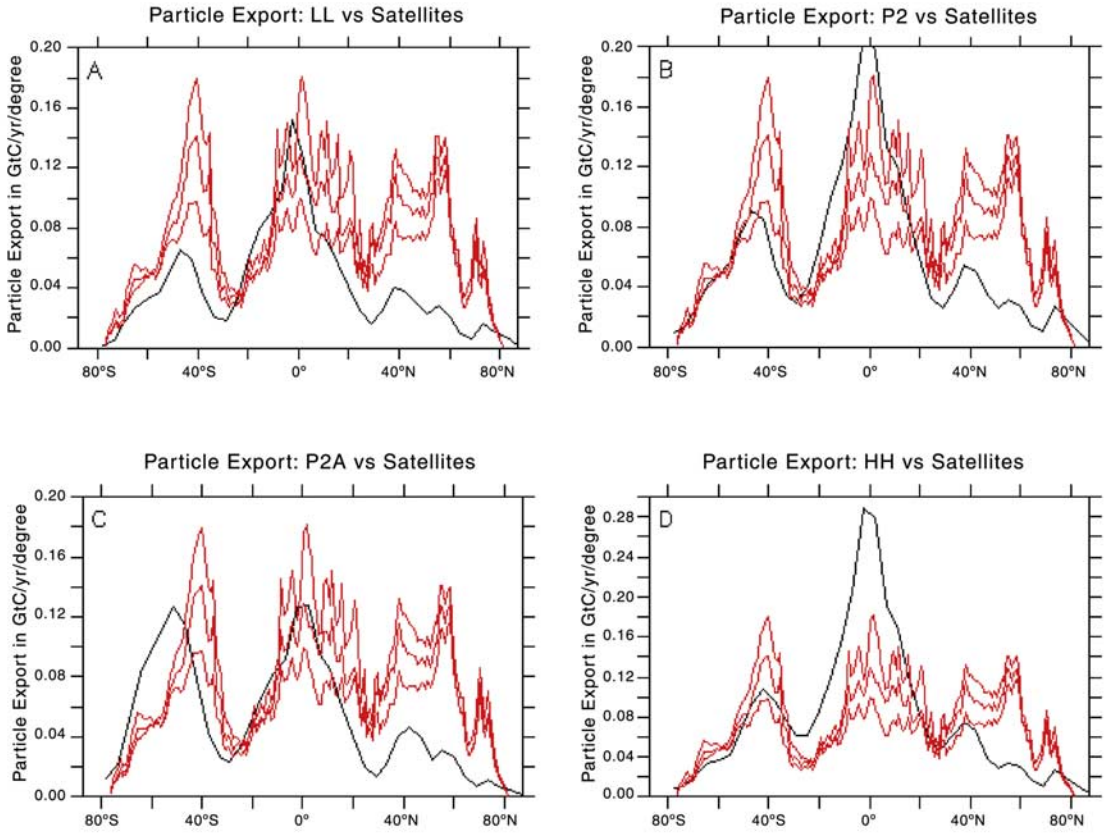

Figure 7. Comparison of observational estimates and models of particle export. Dashed lines are the observational estimates. Solid lines are the models. (a) LL. Note that this model is roughly in the right range in the tropics, but lies below the observational estimates outside the tropics. (b) P2. This model is higher than observations in the tropics, close to the Marra curve in the Southern Ocean, and too low in the north. (c) P2A. Note the displacement of the Southern Ocean export in this simulation. (d) HH. Vertical axis is extended. Note that the tropical production is now severely overestimated.

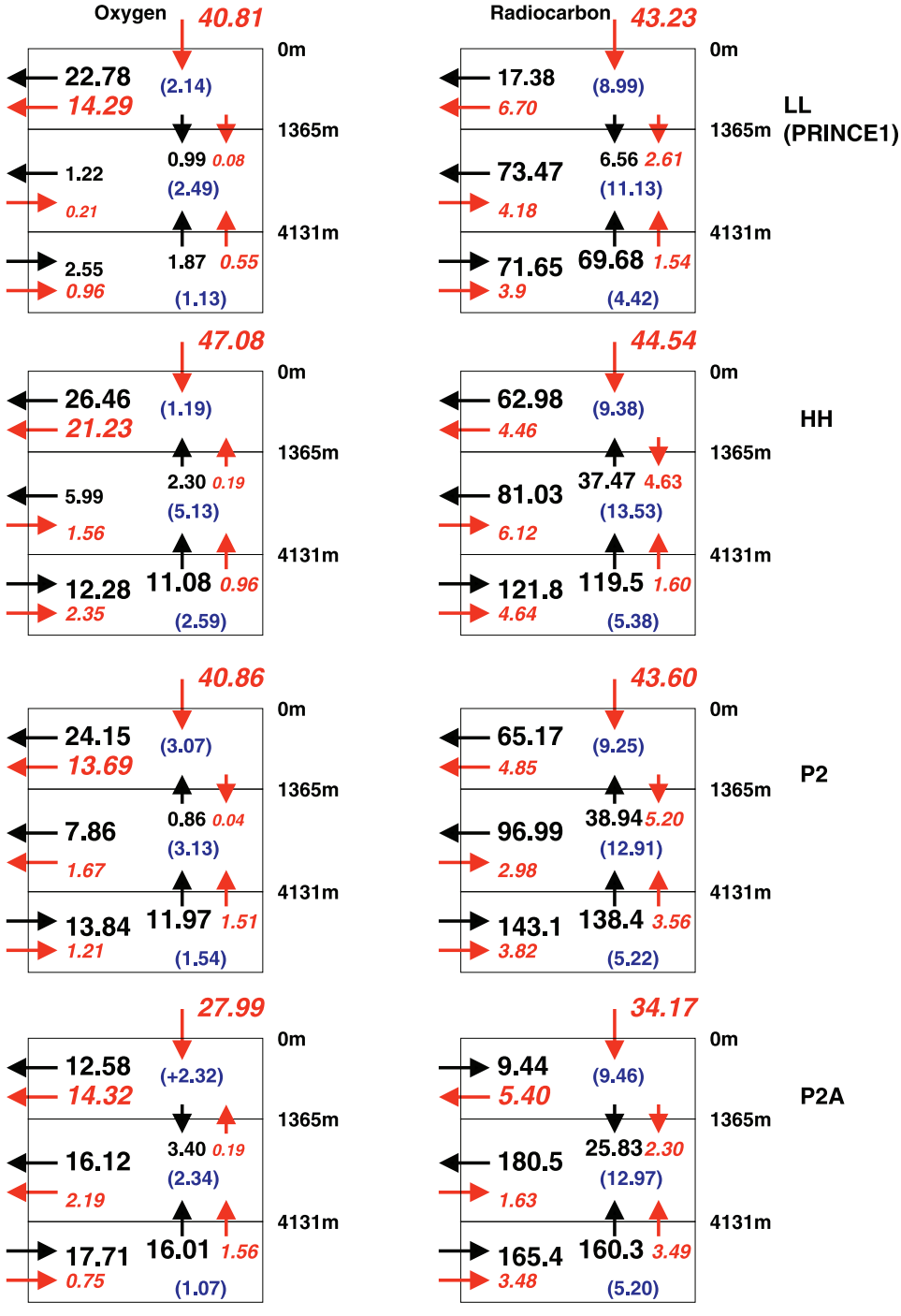

Figure 10. Budgets of oxygen (in Tmol/yr) and radiocarbon (in mol/yr) in the North Pacific (north of 25°N) in four models. Advective fluxes are in black, diffusive are in red, and consumption terms are in blue.

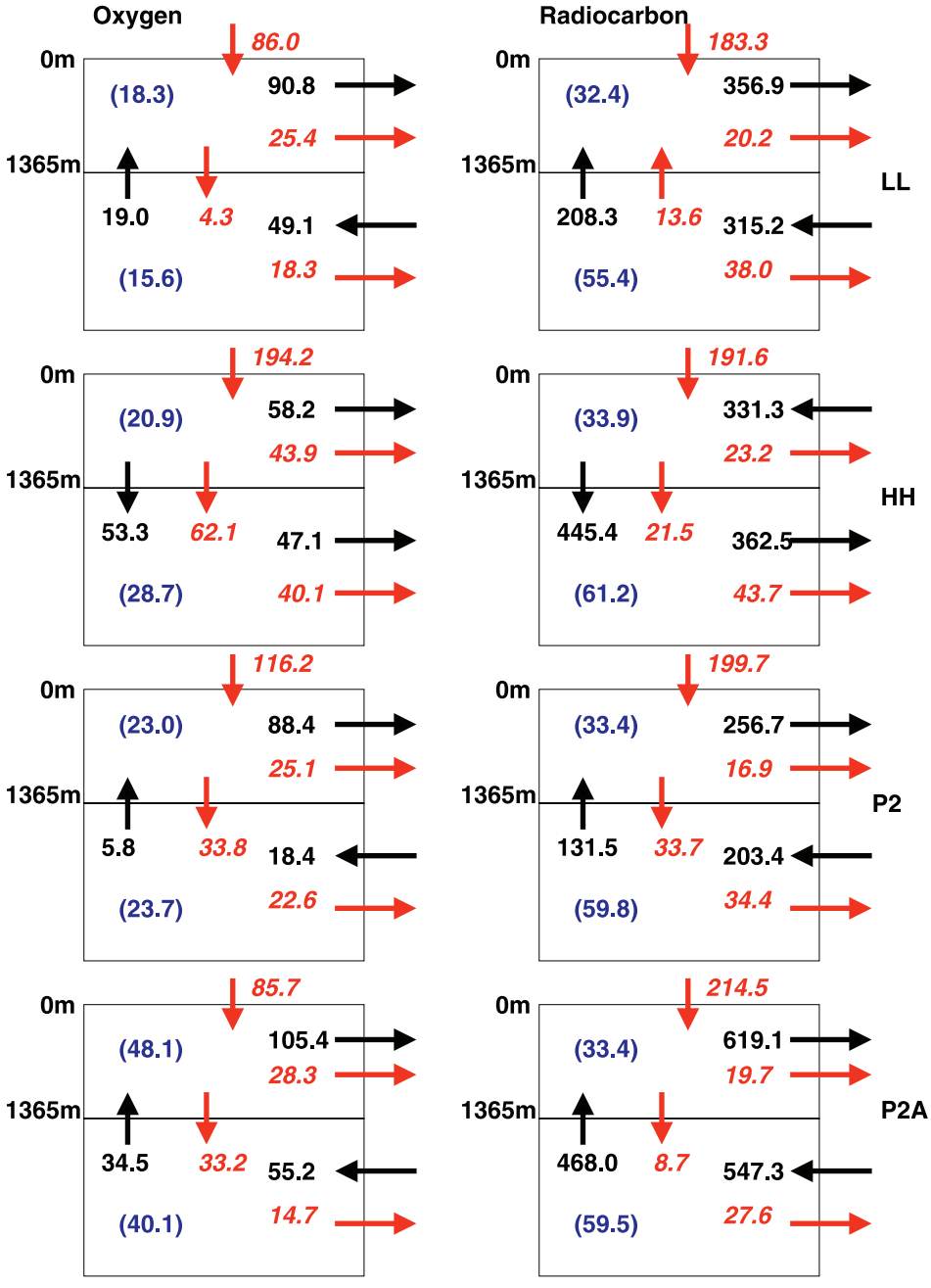

Figure 11. Budgets of oxygen (in Tmol/yr) and radiocarbon (in mol/yr) within the Southern Ocean in four models.

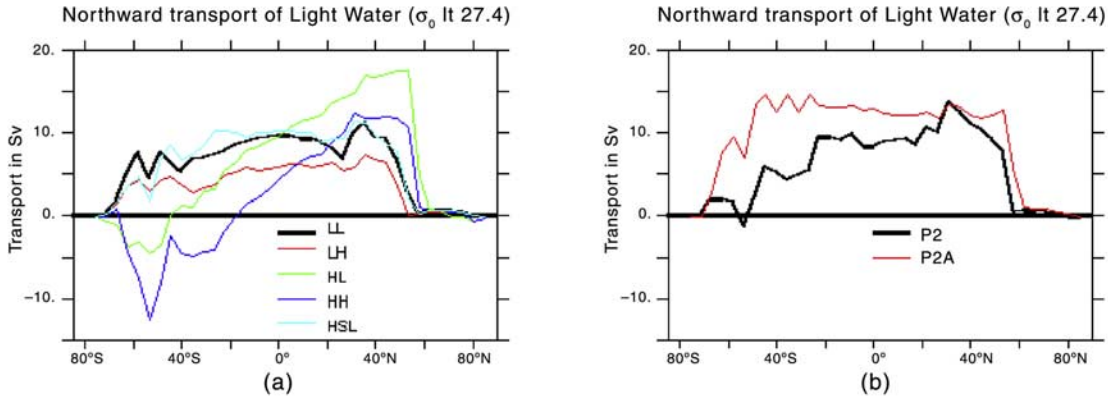

Figure 12. Northward transport of water with σ_θ less than 27.4. Increasing values to the right mean that dense water is being converted to light water. Decreasing values to the right mean that light water is being converted to dense water. (a) Models LL (black), LH (red), HL (green), HH (dark blue), and HSL (light blue). Note that the models with high pycnocline mixing (HH and HL) slope upward to the right across the tropics, indicating that dense water is being converted to light water there. Note also the relatively small difference between HSL and LL. (b) Models P2 and P2A. Note that model P2 is intermediate between LL and HH, having some slope in the tropics. Model P2A has virtually none as the stronger Southern Ocean winds drive a more uniform northward transport.

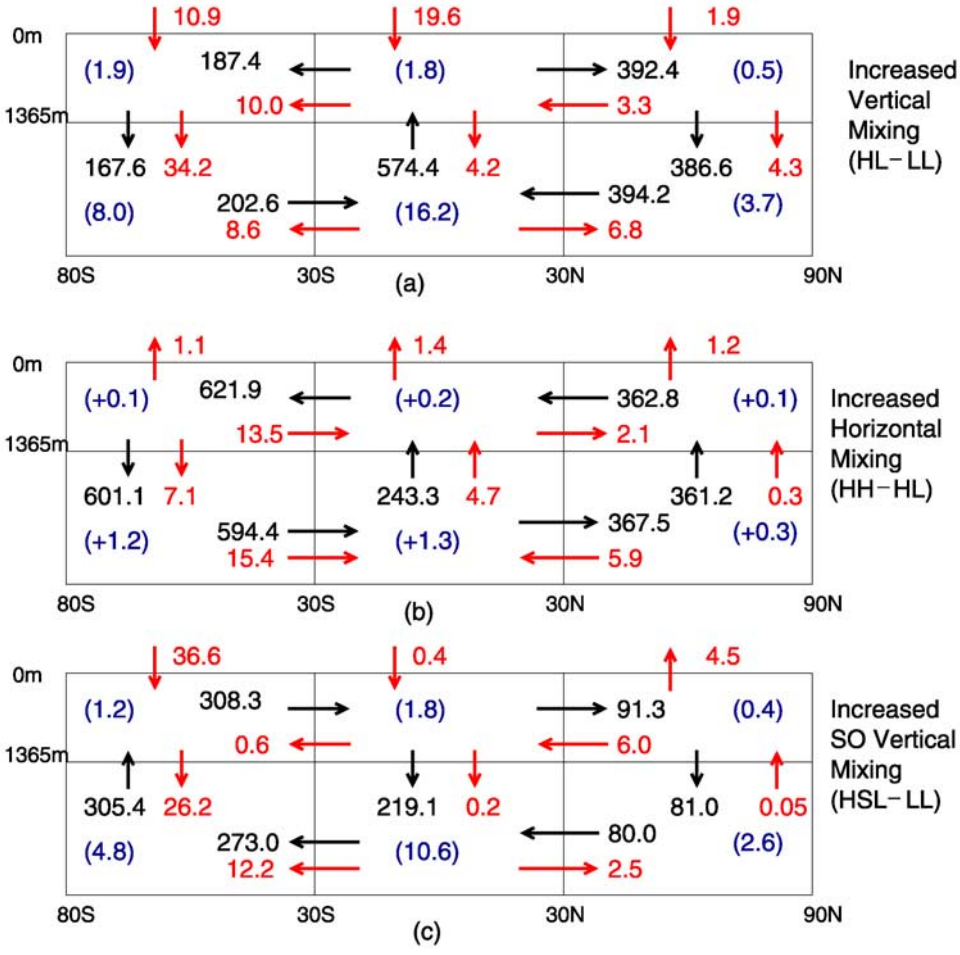

Figure 13. Sensitivity of zonally averaged radiocarbon budget to different parameterizations of mixing (in mol/yr). Note that as before, certain regions are out of balance due to decadal transients. (a) Increase in the vertical mixing (difference between HL and LL). (b) Increase in the lateral mixing (difference between HH and HL). (c) Increase in vertical mixing within the Southern Ocean only (difference between HSL and LL).

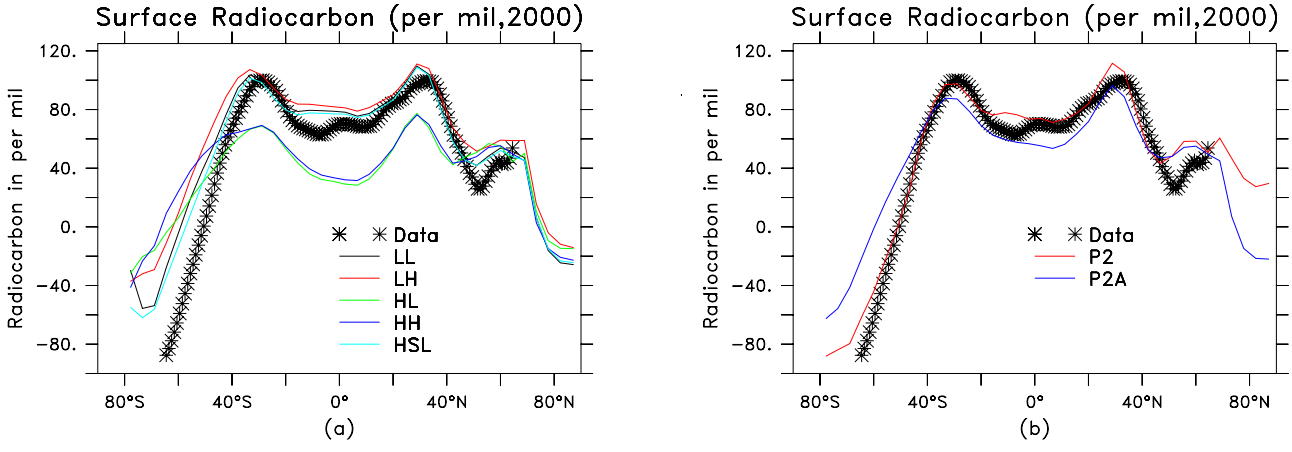

Figure 14. Zonally averaged surface radiocarbon values for models (lines) and data (stars). (a) GSGS model suite. (b) Models P2 and P2A. Note that P2 does the best job at reproducing surface values (which include a bomb component).